Systematic investigation of the link between enzyme catalysis and cold adaptation

Authors:

Catherine D. Stark[1,2], Teanna Bautista-Leung[1], Joanna Siegfried[1], Daniel Herschlag[1, 2, 3]

Affiliations:

[1] Department of Biochemistry, Stanford University, Stanford, California 94305, United States.

[2] ChEM-H, Stanford University, Stanford, California 94305, United States.

[3] Department of Chemical Engineering, Stanford University, Stanford, California 94305, United States.

Abstract

Cold temperature is prevalent across the biosphere and slows the rates of chemical reactions. Increased catalysis has been predicted to be a general adaptive trait of enzymes to reduced temperature, and this expectation has informed physical models for enzyme catalysis and influenced bioprospecting strategies. To broadly test rate as an adaptive trait to cold, we paired kinetic constants of 2223 enzyme reactions with their organism's optimal growth temperature (T_{Growth}) and analyzed trends of rate as a function of T_{Growth}. These data do not support a prevalent increase in rate in cold adaptation. In the model enzyme ketosteroid isomerase (KSI), there was prior evidence for temperature adaptation from a change in an active site residue that results in a tradeoff between activity and stability. Here, we found that little of the overall rate variation for 20 KSI variants was accounted for by T_{Growth}. In contrast, and consistent with prior expectations, we observed a correlation between stability and T_{Growth} across 433 proteins. These results suggest that temperature exerts a weaker selection pressure on enzyme rate than stability and that evolutionary forces other than temperature are responsible for the majority of enzymatic rate variation.

Introduction

Temperature is a ubiquitous environmental property and physical factor that affects the evolution of organisms and the properties and function of the molecules within them. As reaction rates are reduced at lower temperatures (Arrhenius, 1889; Wolfenden et al., 1999), the maintenance of enzyme rates has been suggested to be a universal challenge for organisms at colder temperatures that do not regulate their internal temperature (D'Amico et al., 2003; Fields et al., 2015; Siddiqui and Cavicchioli, 2006; Zecchinon et al., 2001). According to the rate compensation model of temperature adaptation, this challenge is met by cold-adapted enzyme variants providing more rate enhancement than the corresponding warm-adapted variants (Figure 1A). This model predicts that cold-adapted variants are faster than warm-adapted variants when assayed at a common temperature (Figure 1B). Indeed, this behavior has been reported for diverse enzymes, and these observations have been taken as support for this model (Figure 1C, Figure 1D) (Collins and Gerday, 2017; Feller and Gerday, 1997; Siddiqui and Cavicchioli, 2006; Smalås et al., 2000).

The observed rate effects (Figure 1C, Figure 1D) have also led to proposals of general physical models for cold adaptation linked to flexibility, as outlined in Supplementary file 1 (Åqvist et al., 2017; Arcus et al., 2016; Nguyen et al., 2017; Saavedra et al., 2018). Further, features identified in comparative structural analyses of cold and warm-adapted enzymes, such as fewer surface hydrogen bonds and salt bridges (Cai et al., 2018), have been suggested to increase flexibility and thus increase catalysis (Mandelman et al., 2019; H. J. Park et al., 2018; S.-H. Park et al., 2018). Correspondingly, the study of cold adaptation may have the potential to provide generalizable insights into physical properties of enzymes that make them better catalysts, a longstanding challenge in the field (Blow, 2000; Hammes et al., 2011; Kraut et al., 2003; Ringe and Petsko, 2008). From a practical perspective, the prediction of enhanced catalysis by cold-adapted enzymes has motivated low-temperature bioprospecting for biocatalysts to use in industrial processes (Bhatia et al., 2021; Bruno et al., 2019; Kuddus, 2018; Santiago et al., 2016).

Given the theoretical and practical implications of the proposed relationship between enzyme rate and organism growth temperature, we sought to test the generality of the rate compensation model of temperature adaptation. We collated enzyme rate data (Chang et al., 2021) and organism optimal growth temperature (T_{Growth}) (Engqvist, 2018) for 2223 reactions using public databases. The results revealed no enrichment of faster reactions with colder growth

temperatures, and thus did not support increased rate with decreasing environmental temperature as a prevalent adaptation in nature. Further, we found that most rate variation for the enzyme ketosteroid isomerase (KSI) is not accounted for by T_{Growth} despite strong prior evidence for temperature adaptation within its active site (Pinney et al., 2021). In contrast, a similar broad analysis revealed that stability correlates with T_{Growth}, as expected. Our results suggest that temperature exerts a weaker selection pressure on enzyme rate than stability and that other evolutionary forces are responsible for most enzymatic rate variation.

Results

Broadly testing the rate compensation model

To investigate temperature adaptation of enzyme rate, we paired rate data from the BRENDA database (Chang et al., 2021) to organism growth temperatures. We simplified organism temperatures that may span changing conditions (Doblin and van Sebille, 2016) by matching the species name associated with the enzyme variant with the organism optimal growth temperature (T_{Growth}) (Engqvist, 2018). Of 76,083 k_{cat} values in BRENDA, we found that 49,314 were for wild-type enzymes. Of these data, 16,543 values matched to microorganisms with known T_{Growth} values. We selected reactions in the database with variants from more than one organism, spanning 7086 k_{cat} values for 2223 reactions across 815 organisms with at least two variants per reaction (Figure 2A). These reactions spanned a temperature range of 1˚C to 83˚C (Figure 2B).

For each enzyme reaction, we first calculated the rate ratio (k_{cold}/k_{warm}) between the rate of the variant from the lowest growth temperature organism and the rate of the variant from the highest growth temperature organism. We observed rate ratios greater than one (1142 reactions) as predicted by rate compensation, but nearly the same number of rate ratios of less than one (1082 reactions) (Figure 2C, *cf.* Figure 1D), providing no support for widespread or predominant rate compensation.

We also considered the distributions of rate ratios separated by assay temperature (25˚C or 37˚C; Figure 2—figure supplement 1A, 1B) and for wider T_{Growth} ranges (>Δ20˚C or >Δ60˚C; Figure 2—figure supplement 1C, 1D) to assess whether trends were obscured by mixed assay temperatures or narrow T_{Growth} ranges. However, no temperature-dependent trends emerged, supporting the above conclusion of an absence of widespread rate compensation.

To derive a control distribution, we compared enzyme variant rates originating from different organisms with identical T_{Growth} values. We found 615 reactions with more than one variant assigned the same T_{Growth}, and we calculated the rate ratio and its reciprocal (k_{max}/k_{min} and k_{min}/k_{max}) for each reaction. This control distribution (dashed line, Figure 2D) was indistinguishable from the data distribution of rate ratios across T_{Growth} (solid line, Figure 2D; p = 0.21, Mann–Whitney U test, two-sided). Analogous analyses of k_{cat}/K_M values lead to the same conclusions (Figure 2—figure supplement 2).

As it is not possible to prove the absence of a relationship (Altman and Bland, 1995), we examined the slope (m_{rate}) of k_{cat} values *vs.* T_{Growth} for each of the 951 reactions with >2 variants (Figure 2D, Figure 2E, Figure 2—figure supplement 3) to address whether there might be a limited set of enzyme reactions exhibiting significant cold adaptation through a mechanism of enhanced rate. We found two reactions (triose-phosphate isomerase with glyceraldehyde 3-phosphate and cutinase with 4-nitrophenyl butyrate) significantly but positively associated with T_{Growth} (Bonferroni correction; p-value < 5.3×10^{-5}, n = 951).

In summary, the data provide no indication of rate increase as a consequence of decreasing T_{Growth}. These results suggest that rate compensation is not a universal or prevalent consequence of temperature adaptation.

Testing the rate compensation model for the enzyme ketosteroid isomerase (KSI)

To probe rate compensation in greater depth, we turned to the enzyme KSI for which recent data has demonstrated rate compensation (Pinney et al. 2021). Specifically, the change of a single active site residue at position 103 from serine (S103, prevalently found in warm-adapted KSI variants) to protonated aspartic acid (D103, prevalently found in mesophilic KSI variants) provided improved activity from a stronger hydrogen bond while also sacrificing stability by introducing an unfavorable protonation coupled to folding. We therefore used KSI to more deeply investigate the potential for rate compensation by assaying 20 variants that vary in sequence and T_{Growth} (Figure 3A).

KSI catalyzes the double bond isomerization of steroid substrates (Figure 3B) and is predicted to be part of a pathway that enables degradation of steroids for energy and carbon metabolism in bacteria (Horinouchi et al., 2010). KSI variants were identified by sequence relatedness to known KSIs. The 20 selected KSI variants ranged between 20–75% percent

sequence identity to each other (Figure 3—figure supplement 1) and were selected from bacteria originating from environments spanning glaciers, ocean floor, soil, and wastewater with reported T_{Growth} values from 15°C to 46°C (Figure 3—source data 1). Each purified KSI demonstrated similar circular dichroism spectra at 5°C and 25°C, suggesting that variants were not unfolding at the 25°C assay temperature (Figure 3—figure supplement 2). All putative KSI variants exhibited isomerase activity on the steroid substrate 5(10)-estrene-3,17-dione (5(10)-EST) (Figure 3C).

We observed that the KSIs with the prevalent cold-adapted residue (D103 and the similar residue E103, *P. putida* numbering) were not uniformly faster than other KSIs in k_{cat} (Figure 3C) or k_{cat}/K_M (Figure 3—figure supplement 3). The observation that one of the fastest variants contained serine at this position suggests that there are additional factors that influence its rate (Figure 3C & see Discussion).

For KSI, the value of k_{cat} decreased as a function of T_{Growth}, but the shallow slope (m_{rate} = -0.006, p = 0.02) (Figure 3D) and the small coefficient of determination (R^2 = 0.01) of this relationship indicate that T_{Growth} accounts for little of the observed 80-fold rate variation. Similar activity trends were observed at an assay temperature of 15°C (Figure 3—figure supplement 3).

Testing stability compensation using literature data

The absence of evidence for rate compensation led us to reinvestigate the widely accepted relationship between stability and growth temperature. Prior work has shown that temperature optima for observed enzyme rates correlate well with organism T_{Growth} (r = 0.75, (Engqvist, 2018)), but enzyme temperature optima reflect a combination of rate and stability effects. To isolate stability, we surveyed the relationship between stability and T_{Growth} using the ProThermDB, a collection of experimental data of protein and mutant stability (Nikam et al., 2021). Across 433 wild-type variants present in this database, we observed a significant relationship between T_m and T_{Growth} (Figure 4A, R^2 = 0.43, p = 2 x 10^{-54}). For the 43 protein families with more than one reported variant, 39 had a higher melting temperature than their cold-adapted counterpart (Figure 4B).

Discussion

Enzymes have been widely posited to adapt to reduced temperature by increasing rate (Figure 1) (Collins and Gerday, 2017; D'Amico et al., 2003; Siddiqui and Cavicchioli, 2006; Zecchinon et al., 2001). Our results do not support this intuitive and common model as we found that cold-adapted enzyme variants are not generally faster than their warm-adapted counterparts. Even though there was prior evidence for temperature adaptation of the enzyme KSI that is accompanied by rate effects, we found that little of its overall rate variation was accounted for by organismal T_{Growth}, suggesting instead that stability is the dominant driving force underlying the previously identified changes. Our observations suggest that enzyme rate is unlikely to be the primary trait selected for during adaptation to colder environmental temperatures, broadly and in the model system KSI.

Perhaps implicit in the expectation that catalysis will increase in cold adaption is the perspective that faster enzymes are better enzymes, with enzymes reacting at the diffusional limit denoted as "perfect" (Knowles and Albery, 1977). However, most enzymes operate well below the diffusional limit (Bar-Even et al., 2011), underscoring that an *optimal* reaction rate may be different than the *maximal* enzyme rate. There are multiple reasons why optimal or observed enzyme rates may differ from maximal rates. Rate optimization *in vivo* may be accomplished by altering gene expression (Somero, 2004), isoform expression (Somero, 1995), or cellular pH and osmolytes (Hochachka and Lewis, 1971; Yancey and Somero, 1979). Alternatively, the optimal enzyme rate may be lower than the maximal rate to channel metabolites and coordinate metabolism. Further, models of enzyme-metabolite pathway evolution predict that the subset of enzymes that govern pathway flux through rate-limiting steps are under strong rate selection (Noda-Garcia et al., 2018), and it is also possible that maximal enzyme rates are not evolutionarily accessible (Obolski et al., 2018). We speculate that rate compensation may be more probable for highly-related species that live in similar environments, such as marine species that live at different latitudes or depths but otherwise experience little environmental difference (Dong and Somero, 2009).

In contrast to our findings with rate, we observed strong evidence for stability compensation. The temperature dependence of protein unfolding (Becktel and Schellman, 1987) may exert a larger driving force on adaptation than the temperature dependence of rate. There may

be an additional strong selection pressure to avoid unfolded states, as misfolded protein has been demonstrated to have deleterious fitness effects (Geiler-Samerotte et al., 2011) and cells expend considerable energy to clear misfolded variants using chaperones and degradation pathways (Clague and Urbé, 2010; Hartl et al., 2011; Lund, 2001). Additionally, adaptive paths towards stability may be more abundant and more accessible than analogous paths towards rate enhancement, given that each protein may be stabilized individually through a wide variety of mechanisms (Hart et al., 2014) and less constrained by biological context than an enzyme evolving synergistically with complex metabolic networks. The recent discovery of 158,184 positions from 1005 enzyme families that vary with growth temperature may further expand our understanding of the molecular strategies that underlie protein stabilization (Pinney et al., 2021).

The observation that one of the fastest KSIs contains the stabilizing but slowing active site residue, S103 (msKSI, Figure 3C), may illustrate some of the evolutionary complexity alluded to above. As observed with other KSIs, the S103D mutation in msKSI increases activity and decreases stability. However, in msKSI, the decreased stability from the S103D mutation renders it partially unfolded even in the absence of denaturants (Pinney et al., 2021). This result suggests a model where drift or other factors have led to an overall destabilized scaffold, such that msKSI cannot accommodate the activating S103D change (without unfolding) and has made other as yet unidentified amino acid changes that increase activity.

Flexibility has been posited to mechanistically link rate and stability, with multiple underlying interconnections discussed (see Supplementary file 1) (Åqvist et al., 2017; Arcus et al., 2016; D'Amico et al., 2003; Nguyen et al., 2017; Saavedra et al., 2018). Nevertheless, there are many degrees of freedom in an enzyme and most motions are not expected to be coupled to the enzyme reaction coordinate. Our observation of the absence of widespread rate compensation to temperature in contrast to observed stability compensation is consistent with this perspective, as are prior examples of enzyme stabilization in the absence of detrimental rate effects (Minges et al., 2020; Miyazaki et al., 2000; Siddiqui, 2017; Wintrode and Arnold, 2001; Zhao and Feng, 2018). A more complex relationship between these traits seems likely and underscores the need to relate individual and coupled atomic motions to overall flexibility, catalysis, and stability to unravel their intricate interconnections.

To understand why enzyme properties such as rate and stability measured with purified enzymes vary across organisms, we will need to determine their effects on fitness across biological

and environmental contexts. Such studies may synergistically deepen our understanding of enzyme function, organismal evolution, and ecosystems.

Acknowledgments

We thank M. Pinney, H. McShea, D. Mokhtari, C. Markin, I. N. Zheludev, J. Cofsky, E. E. Duffy and members of the Herschlag lab for thought-provoking discussions and review of this manuscript. We also thank F. Sunden, A. Chu, I. N. Zheludev, and F. Yabukarski experimental assistance and B. Eskildsen and D. Mokhtari for computational assistance. This research was supported by NSF Grant MCB-1714723, Stanford ChEM-H Chemistry-Biology Interface Training Program, and an NSF Graduate Research Fellowship to C.D.S and an NSF RET Supplement to J.S.

Materials and Methods

Literature Enzyme Rate Analysis

To capture enzyme rates reported throughout the literature, the BRENDA database was accessed using SOAP July 2021 (Chang et al., 2021) (www.brenda-enzymes.org) and the k_{cat} and k_{cat}/K_M database entries retrieved by Enzyme Commission (E.C.) number were parsed for measurement value, substrate, rate, assay temperature, and variant (wild-type or mutant) status (Source Code 1). Microbial optimum growth temperature (Engqvist 2018) values from median organism optimal growth temperatures for microbes in culture (T_{Growth}) were matched by organism name to rate entries. Rate data were filtered for k_{cat} and k_{cat}/K_M values of wild type enzymes. Reactions are defined by E.C. number–substrate pair. The median value was taken in the case of multiple measurements of the same enzyme variant with the same substrate.

The rate ratio k_{cold}/k_{warm} per reaction was determined by dividing rate of the enzyme from the organism with the minimum T_{Growth} by the rate of the enzyme from organism with the maximum T_{Growth}. If a maximum or minimum T_{Growth} was shared between enzyme variants, then the median rate of the two variants was used in the rate ratio calculation. To account for enzyme rate variation arising independently of temperature, a control distribution from reactions with variants of the same T_{Growth} was derived. The fold change of the maximum value over the minimum value k_{max}/k_{min} and its reciprocal k_{min}/k_{max} was calculated for each reaction from the same T_{Growth} with at least two variants. To compare the rate ratio distribution of the data to the rate ratio control, the nonparametric two-sided Mann–Whitney U test was used with a significance threshold of $p < 0.05$. As no temperature-dependent trends emerged when data were restricted to measurements made at 25˚C or 37˚C or when the T_{Growth} range was limited to >Δ20˚C and >Δ60˚C, we used all data in the main analysis. We determined confidence intervals of the median parameters of the rate ratio distributions by bootstrap analysis (boot package in R, 10,000 replications) (Canty and Ripley, 2021; Davison and Hinkley, 1997). The m_{rate} values (slopes) per reaction were calculated by performing a linear regression relating the $\log_{10}$(rate) *vs*. organism T_{Growth}. Significance threshold, corrected for multiple tests, was $p < 5.33 \times 10^{-5}$ (Bonferroni correction; $p < 0.05/951$).

252 **KSI Variant Identification, Cloning, Expression, and Purification**

253 Putative ketosteroid isomerases (KSI) variants were identified by sequence relatedness to
254 known KSI variants. Selection of variants was guided by associating putative KSI sequences with
255 T_{Growth} by species (Engqvist, 2018). Seventeen variants were synthesized (GenScript or Twist
256 Biosciences) and cloned (Gibson Assembly Protocol, New England Biolabs or Twist Biosciences)
257 into pET-21(+) vectors. KSI variants were aligned using default parameters of Clustal Omega
258 (Madeira et al., 2019) and the maximum likelihood tree was constructed using IQ-TREE with
259 default parameters (Hoang et al., 2018; Nguyen et al., 2015). The constructs were expressed in *E.*
260 *coli* BL21(DE3) cells and purified as previously described (Kraut et al., 2010).
261
262 **KSI Kinetic Measurements**

263 The KSI substrate 5(10)-estrene-3,17-dione (5(10)EST) was purchased from Steraloids
264 (Newport, RI). Reactions of purified KSIs with 5(10)EST were monitored continuously at 248 nm
265 using a Perkin Elmer Lambda 25 UV/Vis spectrometer with an attached VWR digital temperature
266 controlled circulating water bath (Pinney et al., 2021). Temperatures within the cuvettes were
267 measured post-reaction using a platinum electrode thermistor (Omega Engineering) and the
268 temperature of the circulating water bath was modified to maintain a constant internal cuvette
269 temperature between reactions. Reactions were conducted in 40 mM potassium phosphate buffer,
270 pH 7.2, 1 mM disodium EDTA, with 2% DMSO as a co-solvent to maintain substrate solubility.
271 The kinetic parameters k_{cat} and K_M were determined by fitting the observed initial velocity of each
272 reaction as a function of 5(10)EST concentration (9–600 μM; 6–7 different substrate
273 concentrations per experiment) to the Michaelis–Menten equation. Reported values of k_{cat} and K_M
274 are the average of 3–9 independent experiments with at least two different enzyme concentrations
275 varied by at least 5-fold. Reported errors are the standard deviations of these values.
276
277 **KSI Circular Dichroism (CD)**

278 CD spectra were collected for each KSI variant in 40 mM potassium phosphate buffer, pH
279 7.2, 1mM EDTA, at enzyme concentration 20 μM at 5°C and 25°C. Measurements were made on
280 a J-815 Jasco Spectrophotometer between 190-250 nm at 1 nm bandwidth and 50 nm/min scanning
281 speed in a 0.1 cm cuvette (Hellma Analytics).
282

283 **Literature Stability Analysis**

284 Wild-type mutation type stability data were downloaded from ProThermDB (Nikam et al.,
285 2021) with the following fields: protein information (entry, source, mutation, E.C. number),
286 experimental conditions (pH, T, measure, method), thermodynamic parameters (T_m, state,
287 reversibility), and literature (PubMed ID, key words, reference, author). Wild type protein data
288 were matched by species name to microbial optimal growth temperatures T_{Growth} (Engqvist, 2018).
289

References

Altman DG, Bland JM. 1995. Absence of evidence is not evidence of absence. *BMJ* **311**:485. doi:10.1136/bmj.311.7003.485

Åqvist J, Isaksen GV, Brandsdal BO. 2017. Computation of enzyme cold adaptation. *Nat Rev Chem* **1**:0051. doi:10.1038/s41570-017-0051

Arcus VL, Prentice EJ, Hobbs JK, Mulholland AJ, Van der Kamp MW, Pudney CR, Parker EJ, Schipper LA. 2016. On the Temperature Dependence of Enzyme-Catalyzed Rates. *Biochemistry* **55**:1681–1688. doi:10.1021/acs.biochem.5b01094

Arrhenius S. 1889. Über die Dissociationswärme und den Einfluss der Temperatur auf den Dissociationsgrad der Elektrolyte. *Z Für Phys Chem* **4U**:96–116. doi:10.1515/zpch-1889-0408

Bar-Even A, Noor E, Savir Y, Liebermeister W, Davidi D, Tawfik DS, Milo R. 2011. The Moderately Efficient Enzyme: Evolutionary and Physicochemical Trends Shaping Enzyme Parameters. *Biochemistry* **50**:4402–4410. doi:10.1021/bi2002289

Becktel WJ, Schellman JA. 1987. Protein stability curves. *Biopolymers* **26**:1859–1877. doi:10.1002/bip.360261104

Bhatia RK, Ullah S, Hoque MZ, Ahmad I, Yang Y-H, Bhatt AK, Bhatia SK. 2021. Psychrophiles: A source of cold-adapted enzymes for energy efficient biotechnological industrial processes. *J Environ Chem Eng* **9**:104607. doi:10.1016/j.jece.2020.104607

Blow D. 2000. So do we understand how enzymes work? *Struct Lond Engl 1993* **8**:R77-81. doi:10.1016/s0969-2126(00)00125-8

Bruno S, Coppola D, di Prisco G, Giordano D, Verde C. 2019. Enzymes from Marine Polar Regions and Their Biotechnological Applications. *Mar Drugs* **17**:544. doi:10.3390/md17100544

Cai Z-W, Ge H-H, Yi Z-W, Zeng R-Y, Zhang G-Y. 2018. Characterization of a novel psychrophilic and halophilic β-1, 3-xylanase from deep-sea bacterium, Flammeovirga pacifica strain WPAGA1. *Int J Biol Macromol* **118**:2176–2184. doi:10.1016/j.ijbiomac.2018.07.090

Canty A, Ripley BD. 2021. boot: Bootstrap R (S-Plus) Functions.

Chang A, Jeske L, Ulbrich S, Hofmann J, Koblitz J, Schomburg I, Neumann-Schaal M, Jahn D, Schomburg D. 2021. BRENDA, the ELIXIR core data resource in 2021: new developments and updates. *Nucleic Acids Res* **49**:D498–D508. doi:10.1093/nar/gkaa1025

Clague MJ, Urbé S. 2010. Ubiquitin: Same Molecule, Different Degradation Pathways. *Cell* **143**:682–685. doi:10.1016/j.cell.2010.11.012

Collins T, Gerday C. 2017. Enzyme Catalysis in Psychrophiles In: Margesin R, editor. Psychrophiles: From Biodiversity to Biotechnology. Cham: Springer International Publishing. pp. 209–235. doi:10.1007/978-3-319-57057-0_10

D'Amico S, Marx J-C, Gerday C, Feller G. 2003. Activity-stability relationships in extremophilic enzymes. *J Biol Chem* **278**:7891–7896. doi:10.1074/jbc.M212508200

Davison AC, Hinkley DV. 1997. Bootstrap Methods and Their Applications. Cambridge: Cambridge University Press.

Doblin MA, van Sebille E. 2016. Drift in ocean currents impacts intergenerational microbial exposure to temperature. *Proc Natl Acad Sci U S A* **113**:5700–5705. doi:10.1073/pnas.1521093113

Dong Y, Somero GN. 2009. Temperature adaptation of cytosolic malate dehydrogenases of limpets (genus Lottia): differences in stability and function due to minor changes in

sequence correlate with biogeographic and vertical distributions. *J Exp Biol* **212**:169–177. doi:10.1242/jeb.024505

Engqvist MKM. 2018. Correlating enzyme annotations with a large set of microbial growth temperatures reveals metabolic adaptations to growth at diverse temperatures. *BMC Microbiol* **18**:177. doi:10.1186/s12866-018-1320-7

Feller G, Gerday C. 1997. Psychrophilic enzymes: molecular basis of cold adaptation. *Cell Mol Life Sci CMLS* **53**:830–841. doi:10.1007/s000180050103

Fields PA, Dong Y, Meng X, Somero GN. 2015. Adaptations of protein structure and function to temperature: there is more than one way to "skin a cat." *J Exp Biol* **218**:1801–1811. doi:10.1242/jeb.114298

Geiler-Samerotte KA, Dion MF, Budnik BA, Wang SM, Hartl DL, Drummond DA. 2011. Misfolded proteins impose a dosage-dependent fitness cost and trigger a cytosolic unfolded protein response in yeast. *Proc Natl Acad Sci U S A* **108**:680–685. doi:10.1073/pnas.1017570108

Hammes GG, Benkovic SJ, Hammes-Schiffer S. 2011. Flexibility, Diversity, and Cooperativity: Pillars of Enzyme Catalysis. *Biochemistry* **50**:10422–10430. doi:10.1021/bi201486f

Hart KM, Harms MJ, Schmidt BH, Elya C, Thornton JW, Marqusee S. 2014. Thermodynamic system drift in protein evolution. *PLoS Biol* **12**:e1001994. doi:10.1371/journal.pbio.1001994

Hartl FU, Bracher A, Hayer-Hartl M. 2011. Molecular chaperones in protein folding and proteostasis. *Nature* **475**:324–332. doi:10.1038/nature10317

Hoang DT, Chernomor O, von Haeseler A, Minh BQ, Vinh LS. 2018. UFBoot2: Improving the Ultrafast Bootstrap Approximation. *Mol Biol Evol* **35**:518–522. doi:10.1093/molbev/msx281

Hochachka PW, Lewis JK. 1971. Interacting effects of pH and temperature on the Km values for fish tissue lactate dehydrogenases. *Comp Biochem Physiol Part B Comp Biochem* **39**:925–933. doi:10.1016/0305-0491(71)90116-7

Horinouchi M, Kurita T, Hayashi T, Kudo T. 2010. Steroid degradation genes in Comamonas testosteroni TA441: Isolation of genes encoding a Δ4(5)-isomerase and 3α- and 3β-dehydrogenases and evidence for a 100 kb steroid degradation gene hot spot. *J Steroid Biochem Mol Biol* **122**:253–263. doi:10.1016/j.jsbmb.2010.06.002

Knowles JR, Albery WJ. 1977. Perfection in enzyme catalysis: the energetics of triosephosphate isomerase. *Acc Chem Res* **10**:105–111. doi:10.1021/ar50112a001

Kraut DA, Carroll KS, Herschlag D. 2003. Challenges in enzyme mechanism and energetics. *Annu Rev Biochem* **72**:517–571. doi:10.1146/annurev.biochem.72.121801.161617

Kraut DA, Sigala PA, Fenn TD, Herschlag D. 2010. Dissecting the paradoxical effects of hydrogen bond mutations in the ketosteroid isomerase oxyanion hole. *Proc Natl Acad Sci* **107**:1960–1965. doi:10.1073/pnas.0911168107

Kuddus M. 2018. Cold-active enzymes in food biotechnology: An updated mini review. *J Appl Biol Biotechnol* 58–63. doi:10.7324/JABB.2018.60310

Lund PA. 2001. Microbial molecular chaperones. *Adv Microb Physiol* **44**:93–140. doi:10.1016/s0065-2911(01)44012-4

Madeira F, Park YM, Lee J, Buso N, Gur T, Madhusoodanan N, Basutkar P, Tivey ARN, Potter SC, Finn RD, Lopez R. 2019. The EMBL-EBI search and sequence analysis tools APIs in 2019. *Nucleic Acids Res* **47**:W636–W641. doi:10.1093/nar/gkz268

Mandelman D, Ballut L, Wolff DA, Feller G, Gerday C, Haser R, Aghajari N. 2019. Structural determinants increasing flexibility confer cold adaptation in psychrophilic phosphoglycerate kinase. *Extremophiles* **23**:495–506. doi:10.1007/s00792-019-01102-x

Minges H, Schnepel C, Böttcher D, Weiß MS, Sproß J, Bornscheuer UT, Sewald N. 2020. Targeted Enzyme Engineering Unveiled Unexpected Patterns of Halogenase Stabilization. *ChemCatChem* **12**:818–831. doi:10.1002/cctc.201901827

Miyazaki K, Wintrode PL, Grayling RA, Rubingh DN, Arnold FH. 2000. Directed evolution study of temperature adaptation in a psychrophilic enzyme. *J Mol Biol* **297**:1015–1026. doi:10.1006/jmbi.2000.3612

Nguyen L-T, Schmidt HA, von Haeseler A, Minh BQ. 2015. IQ-TREE: a fast and effective stochastic algorithm for estimating maximum-likelihood phylogenies. *Mol Biol Evol* **32**:268–274. doi:10.1093/molbev/msu300

Nguyen V, Wilson C, Hoemberger M, Stiller JB, Agafonov RV, Kutter S, English J, Theobald DL, Kern D. 2017. Evolutionary drivers of thermoadaptation in enzyme catalysis. *Science* **355**:289–294. doi:10.1126/science.aah3717

Nikam R, Kulandaisamy A, Harini K, Sharma D, Gromiha MM. 2021. ProThermDB: thermodynamic database for proteins and mutants revisited after 15 years. *Nucleic Acids Res* **49**:D420–D424. doi:10.1093/nar/gkaa1035

Noda-Garcia L, Liebermeister W, Tawfik DS. 2018. Metabolite-Enzyme Coevolution: From Single Enzymes to Metabolic Pathways and Networks. *Annu Rev Biochem* **87**:187–216. doi:10.1146/annurev-biochem-062917-012023

Obolski U, Ram Y, Hadany L. 2018. Key issues review: evolution on rugged adaptive landscapes. *Rep Prog Phys Phys Soc G B* **81**:012602. doi:10.1088/1361-6633/aa94d4

Park HJ, Lee CW, Kim D, Do H, Han SJ, Kim JE, Koo B-H, Lee JH, Yim JH. 2018. Crystal structure of a cold-active protease (Pro21717) from the psychrophilic bacterium, Pseudoalteromonas arctica PAMC 21717, at 1.4 Å resolution: Structural adaptations to cold and functional analysis of a laundry detergent enzyme. *PLOS ONE* **13**:e0191740. doi:10.1371/journal.pone.0191740

Park S-H, Yoo W, Lee CW, Jeong CS, Shin SC, Kim H-W, Park H, Kim KK, Kim TD, Lee JH. 2018. Crystal structure and functional characterization of a cold-active acetyl xylan esterase (PbAcE) from psychrophilic soil microbe Paenibacillus sp. *PLOS ONE* **13**:e0206260. doi:10.1371/journal.pone.0206260

Pinney MM, Mokhtari DA, Akiva E, Yabukarski F, Sanchez DM, Liang R, Doukov T, Martinez TJ, Babbitt PC, Herschlag D. 2021. Parallel molecular mechanisms for enzyme temperature adaptation. *Science* **371**:eaay2784. doi:10.1126/science.aay2784

Pollack RM, Bantia S, Bounds PL, Koffman BM. 1986. pH dependence of the kinetic parameters for 3-oxo-.DELTA.5-steroid isomerase. Substrate catalysis and inhibition by (3S)-spiro[5.alpha.-androstane-3,2'-oxiran]-17-one. *Biochemistry* **25**:1905–1911. doi:10.1021/bi00356a011

Ringe D, Petsko GA. 2008. How enzymes work. *Science* **320**:1428–1429. doi:10.1126/science.1159747

Saavedra HG, Wrabl JO, Anderson JA, Li J, Hilser VJ. 2018. Dynamic allostery can drive cold adaptation in enzymes. *Nature* **558**:324–328. doi:10.1038/s41586-018-0183-2

Santiago M, Ramírez-Sarmiento CA, Zamora RA, Parra LP. 2016. Discovery, Molecular Mechanisms, and Industrial Applications of Cold-Active Enzymes. *Front Microbiol* **7**:1408. doi:10.3389/fmicb.2016.01408

Siddiqui KS. 2017. Defying the activity–stability trade-off in enzymes: taking advantage of entropy to enhance activity and thermostability. *Crit Rev Biotechnol* **37**:309–322. doi:10.3109/07388551.2016.1144045

Siddiqui KS, Cavicchioli R. 2006. Cold-Adapted Enzymes. *Annu Rev Biochem* **75**:403–433. doi:10.1146/annurev.biochem.75.103004.142723

Smalås AO, Leiros HK, Os V, Willassen NP. 2000. Cold adapted enzymes. *Biotechnol Annu Rev* **6**:1–57. doi:10.1016/s1387-2656(00)06018-x

Somero GN. 2004. Adaptation of enzymes to temperature: searching for basic "strategies." *Comp Biochem Physiol B Biochem Mol Biol* **139**:321–333. doi:10.1016/j.cbpc.2004.05.003

Somero GN. 1995. Proteins and temperature. *Annu Rev Physiol* **57**:43–68. doi:10.1146/annurev.ph.57.030195.000355

Wintrode PL, Arnold FH. 2001. Temperature adaptation of enzymes: Lessons from laboratory evolutionAdvances in Protein Chemistry. Elsevier. pp. 161–225. doi:10.1016/S0065-3233(01)55004-4

Wolfenden R, Snider M, Ridgway C, Miller B. 1999. The Temperature Dependence of Enzyme Rate Enhancements. *J Am Chem Soc* **121**:7419–7420. doi:10.1021/ja991280p

Yancey PH, Somero GN. 1979. Counteraction of urea destabilization of protein structure by methylamine osmoregulatory compounds of elasmobranch fishes. *Biochem J* **183**:317–323. doi:10.1042/bj1830317

Zecchinon L, Claverie P, Collins T, D'Amico S, Delille D, Feller G, Georlette D, Gratia E, Hoyoux A, Meuwis M-A, Sonan G, Gerday C. 2001. Did psychrophilic enzymes really win the challenge? *Extremophiles* **5**:313–321. doi:10.1007/s007920100207

Zhao H-Y, Feng H. 2018. Engineering Bacillus pumilus alkaline serine protease to increase its low-temperature proteolytic activity by directed evolution. *BMC Biotechnol* **18**:34. doi:10.1186/s12896-018-0451-0

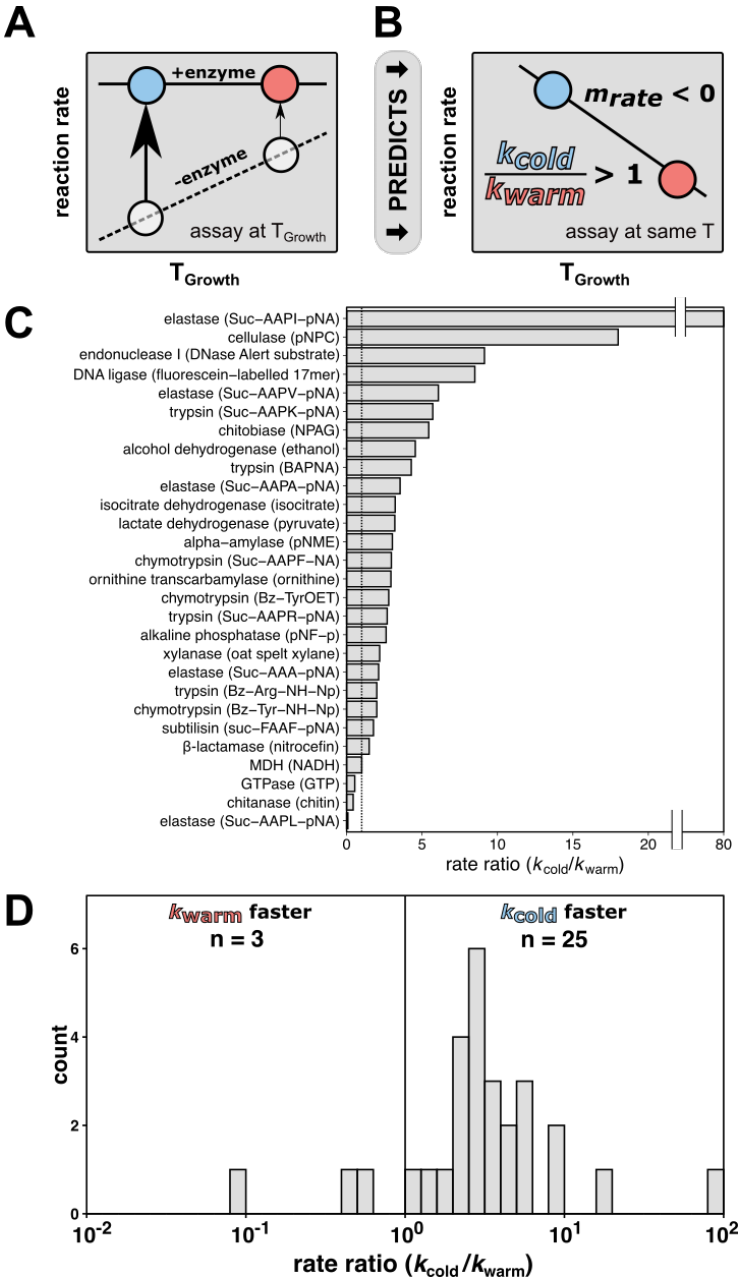

Figure 1: The rate compensation model of cold adaptation predicts that cold-adapted enzymes exhibit greater catalysis and are faster at a common temperature than their warm-adapted counterparts. (A) According to the rate compensation model of cold adaptation, a cold-adapted variant (blue circle) has larger rate enhancement than a warm-adapted variant (red circle). The dashed line represents the uncatalyzed reaction, the solid line represents the catalyzed reaction, and the arrows represent the rate enhancement at the respective organism T_{Growth}. (B) When variants are assayed at a common temperature, rate compensation predicts a faster reaction for the enzyme from the cold-adapted organism, corresponding to a rate ratio (k_{cold}/k_{warm}) of greater than one and a negative slope of rate *vs*. T_{Growth} (m_{rate}). (C, D) Rate comparisons of warm-adapted and cold-adapted enzyme variants made at identical temperatures from cold adaptation literature spanning indicated reactions with substrate specified in parentheses (Collins and Gerday, 2017; Feller and Gerday, 1997; Siddiqui and Cavicchioli, 2006; Smalås et al., 2000). The black vertical lines represents no rate change with temperature (*i.e.,* rate ratio = 1).

Figure 1—source data 1: Figure1_SourceData1.csv

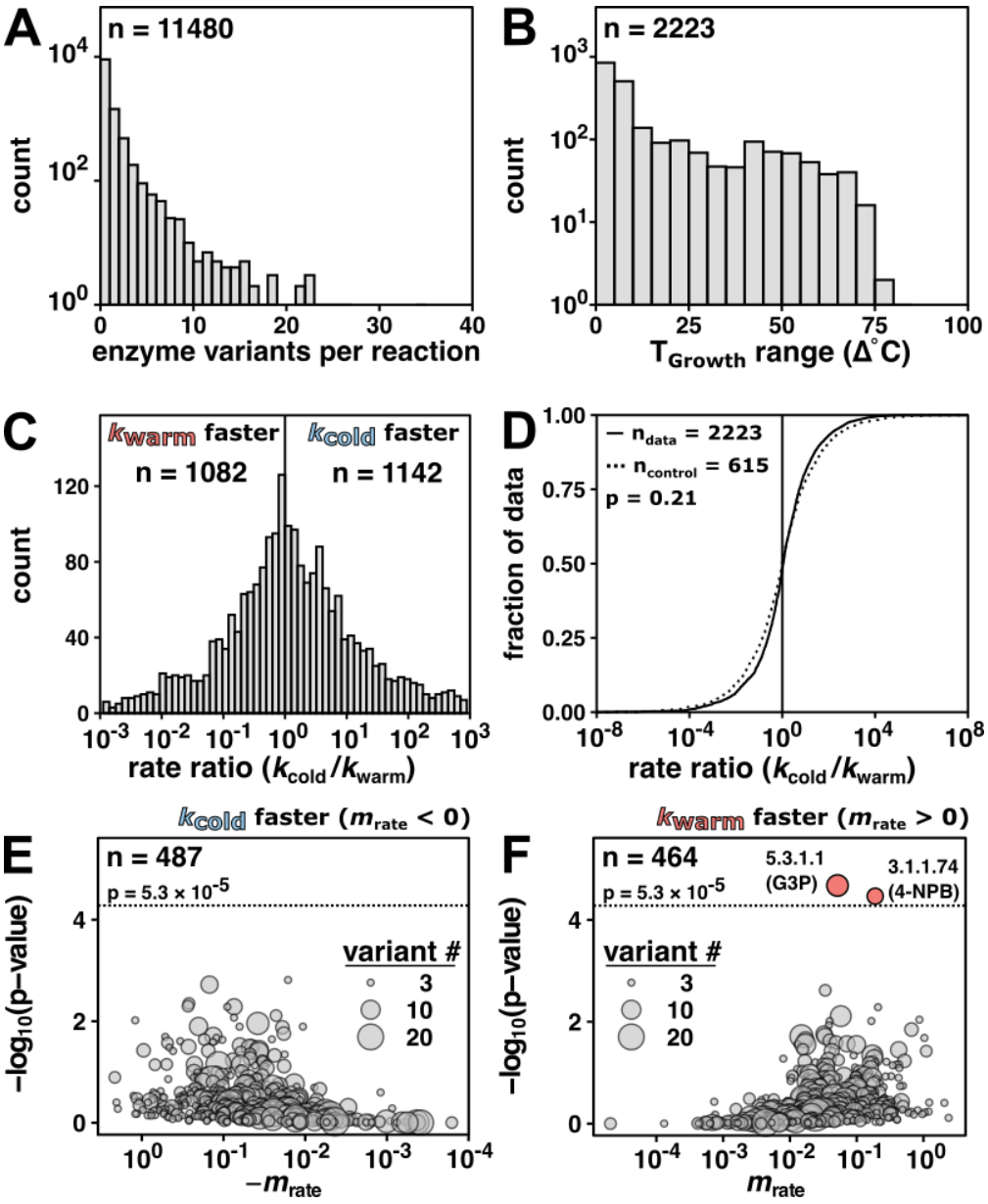

Figure 2: Enzyme rate data (k_{cat}) do not indicate general rate compensation. (A) Enzyme variants per reaction of wild-type enzyme k_{cat} values (n = 11480 reactions) matched to T_{Growth}. (B) Reactions with more than one enzyme variant (n = 2223 reactions). (C) Rate ratio distribution of the rate at the coldest T_{Growth} (k_{cold}) divided by the rate of the variant from the warmest T_{Growth} (k_{warm}) (median = 1.1 fold, 95% CI [1.00, 1.22], n = 2223 reactions). Vertical line at rate ratio = 1. For clarity, only data with rate ratios between 10^{-3} and 10^{3} are shown (>95% of the reactions). (D) Rate ratio (k_{cold}/k_{warm}) data (solid line, n = 2223 from panel C) compared to fold change control distribution (same T_{Growth}; dashed line, median = 1.0 fold, 95% CI [0.89, 1.13], n = 615 reactions; p = 0.21, Mann–Whitney U test, two-sided). The black vertical line represents no rate change with temperature (*i.e.,* rate ratio = 1). (E, F) The significance and magnitude of the linear fit of reaction rate as a function of T_{Growth} for negative slopes (E, n = 487) and positive slopes (F, n = 464) in log space. E.C. number and (substrate) indicated for reactions significantly associated with temperature (Bonferroni correction; p-value < 5.3×10^{-5}, n = 951). Dotted horizontal lines at $p = -\log_{10}(5.3 \times 10^{-5})$. 5.3.1.1: triose-phosphate isomerase; G3P: glyceraldehyde 3-phosphate; 3.1.1.74: cutinase; 4-NPB: 4-nitrophenyl butyrate.

Figure 2—source data 1: Figure2_SourceData1.csv

Figure 2—source data 2: Figure2_SourceData2.csv

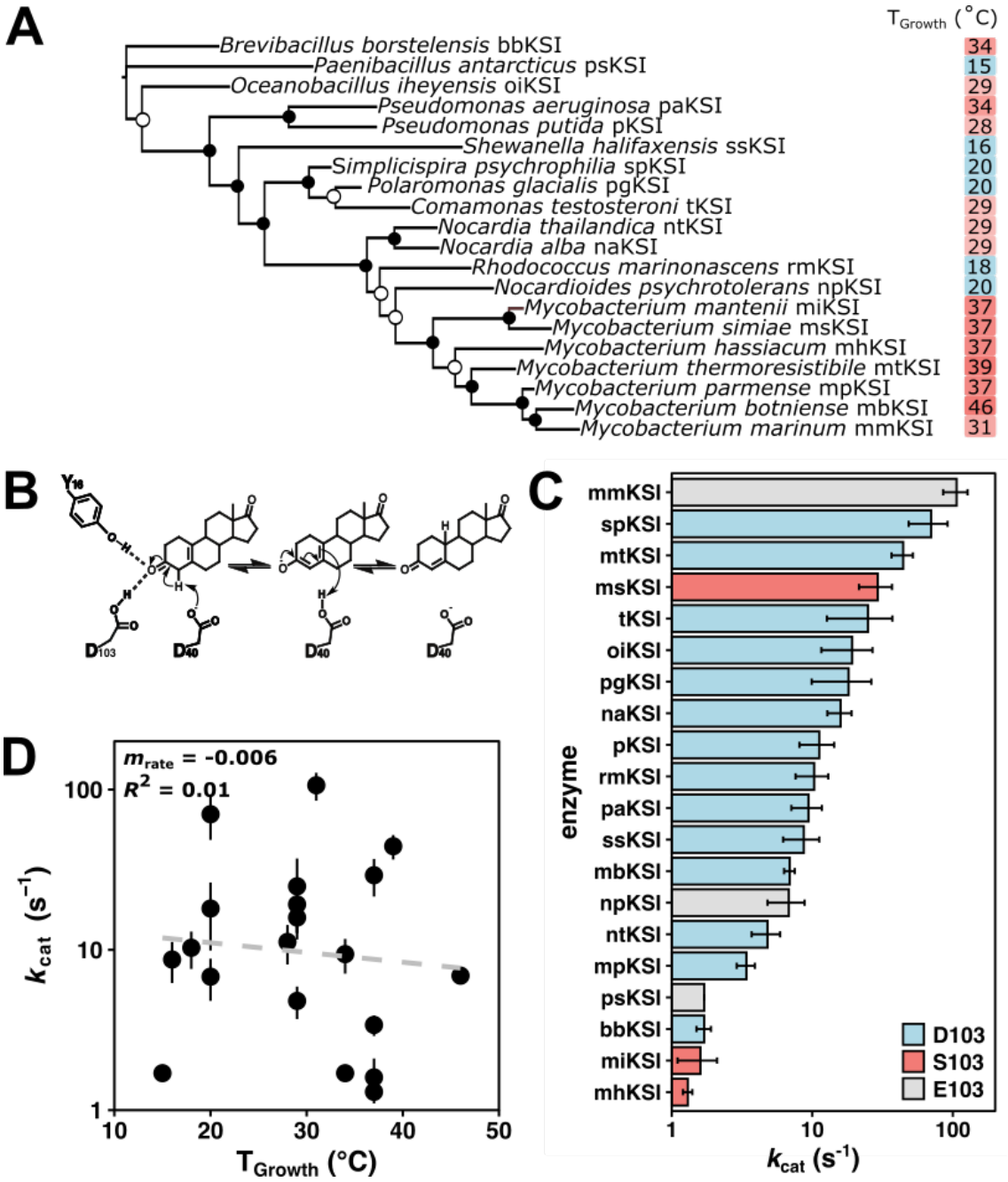

Figure 3: Ketosteroid isomerase (KSI) rates do not indicate rate compensation. (A) Unrooted maximum likelihood phylogenetic tree of KSI variants. Closed circles represent bootstrap values of >70%; open circles represent bootstrap values of 40-70%. (B) The mechanism of isomerization of the steroid 5(10)-estrene-3,17-dione by KSI. 5(10)-EST was used to allow direct measurement of the rate-limiting chemical step k_{cat} (Pollack et al., 1986) (C) Activity of KSI variants (k_{cat}) at a common assay temperature of 25°C. Error bars represent standard deviation of at least two different experimental replicates varying [E] at least five-fold. KSI variants with D103 are represented in blue, S103 in red, and E103 in grey (*P. putida* numbering throughout). (D) Activity ($\log_{10}(k_{cat})$) of KSI variants at a common assay temperature (25°C) *vs.* organism growth temperature (T_{Growth}) (n = 20, m_{rate} = -0.006, R^2 = 0.01, p = 0.02).

Figure 3—source data 1: KSI origins and organism growth temperatures

Figure 3—source data 2: Kinetic measurement of KSIs at 25˚C with substrate 5(10)-estrene-3,17-dione.

Figure 3—source data 3: Kinetic measurement of KSIs at 15˚C with substrate 5(10)-estrene-3,17-dione.

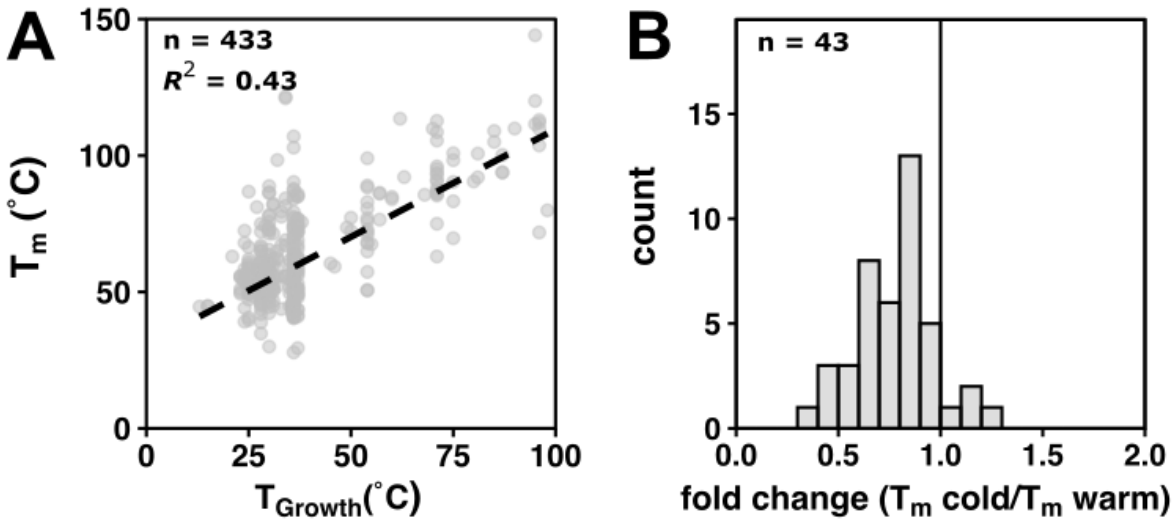

Figure 4: Protein stability data display stability compensation. (A) Wild-type T_m stability data from ProThermDB as a function of organism T_{Growth}. Dashed black line represents a linear fit (n = 433, R^2 = 0.43). (B) Fold change (T_m cold/T_m warm) of wild-type protein variants (n = 43, median = 0.81, 95% [0.70, 0.85]. The black vertical line represents no change (*i.e.,* fold change = 1).

Figure 4—source data 1: Figure4_SourceData1.csv

Figure 4—source data 2: Figure4_SourceData2.csv

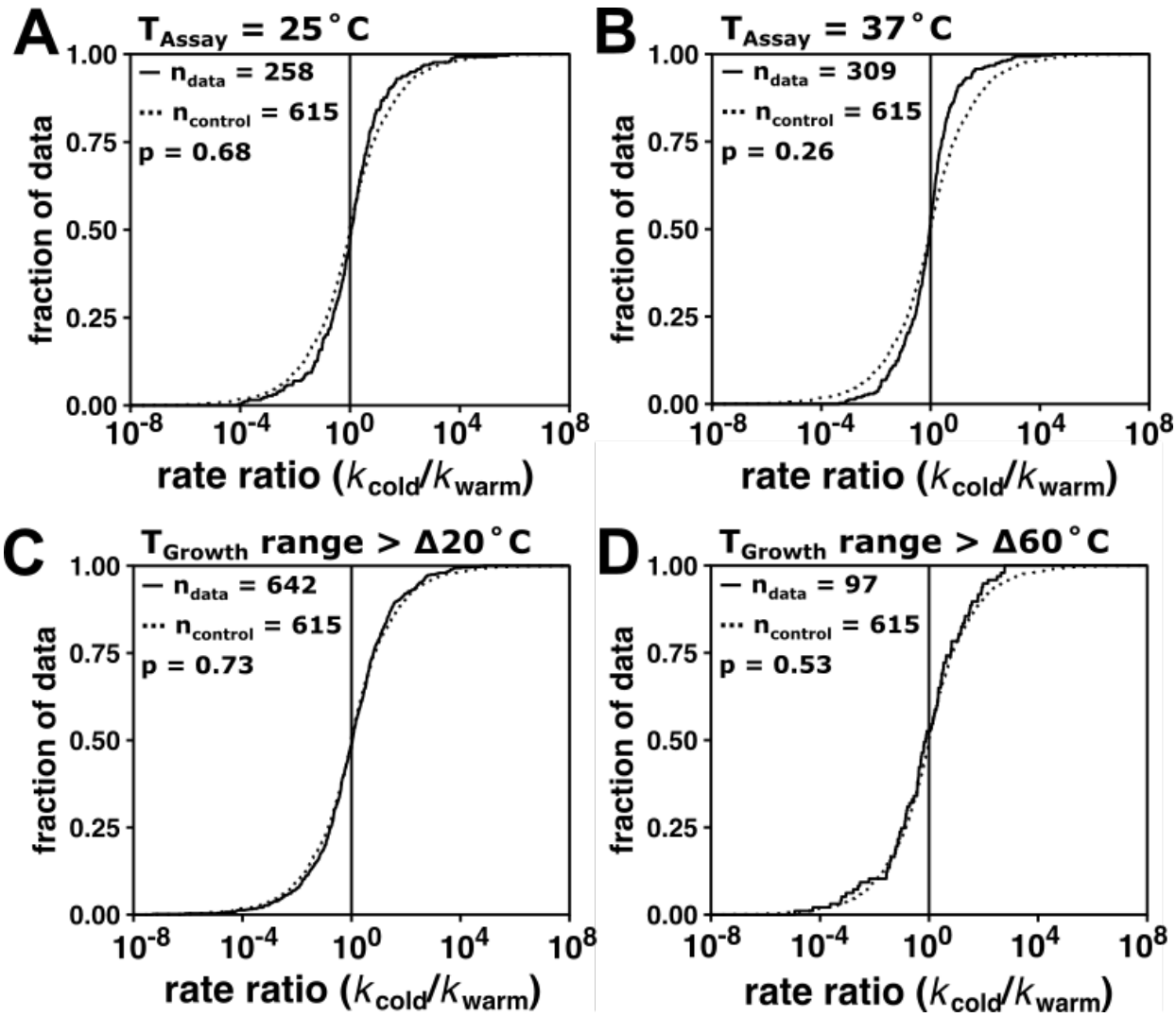

Figure 2—figure supplement 1: Specifying assay temperature and organism optimal growth temperature range per reaction does not alter conclusions.
(A) Distribution of k_{cat} rate ratio values including only measurements made at 25˚C and (B) 37˚C. (C) Distribution of rate ratios with T_{Growth} range > Δ20˚C and (D) T_{Growth} range > 60˚C. Reported p-values from two-sided Mann–Whitney U test comparing filtered data (solid line) and the control data (dotted line, see Materials & Methods).

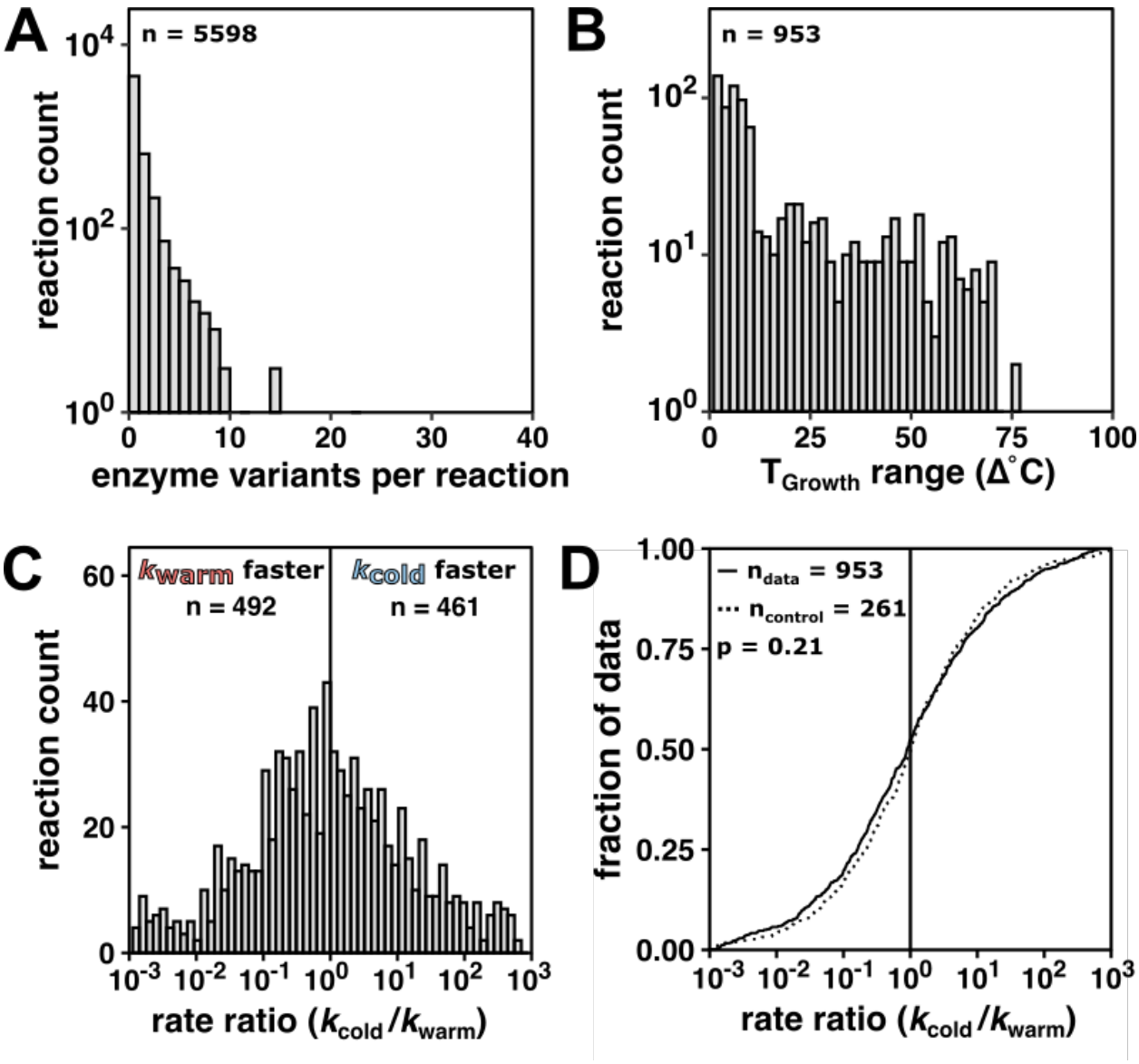

Figure 2—figure supplement 2: Enzyme rate data for k_{cat}/K_M do not indicate rate compensation, supporting the conclusions from the k_{cat} analysis in the main text.

(A) Variants per reaction of wild-type enzyme k_{cat} values (n = 5598 reactions) matched to T_{Growth}. (B) Number of reactions spanning the specified T_{Growth} range (n = 953 reactions with >1 variant). (C) k_{cat}/K_M rate ratio (k_{cold}/k_{warm}) distribution (median = 0.93 fold, 95% CI [0.78, 1.12], n = 953 reactions). Grey vertical line at rate ratio = 1. (D) k_{cat}/K_M rate ratio (k_{cold}/k_{warm}) data (black line, n = 953 reactions) with k_{cat}/K_M rate ratio control (grey line, median = 1.00 fold, 95% CI [0.82, 1.21], n = 307 reactions) determined in the same way as the k_{cat} rate ratio control in the main text (see Materials & Methods) (p = 0.80, Mann–Whitney U test, two-sided). For clarity, only data with rate ratios between 10^{-3} and 10^{3} are shown, representing >90% rate ratio data in (C) and >83% of rate ratio control values in (D). Black vertical line represents no rate change with temperature (*i.e.*, rate ratio = 1).

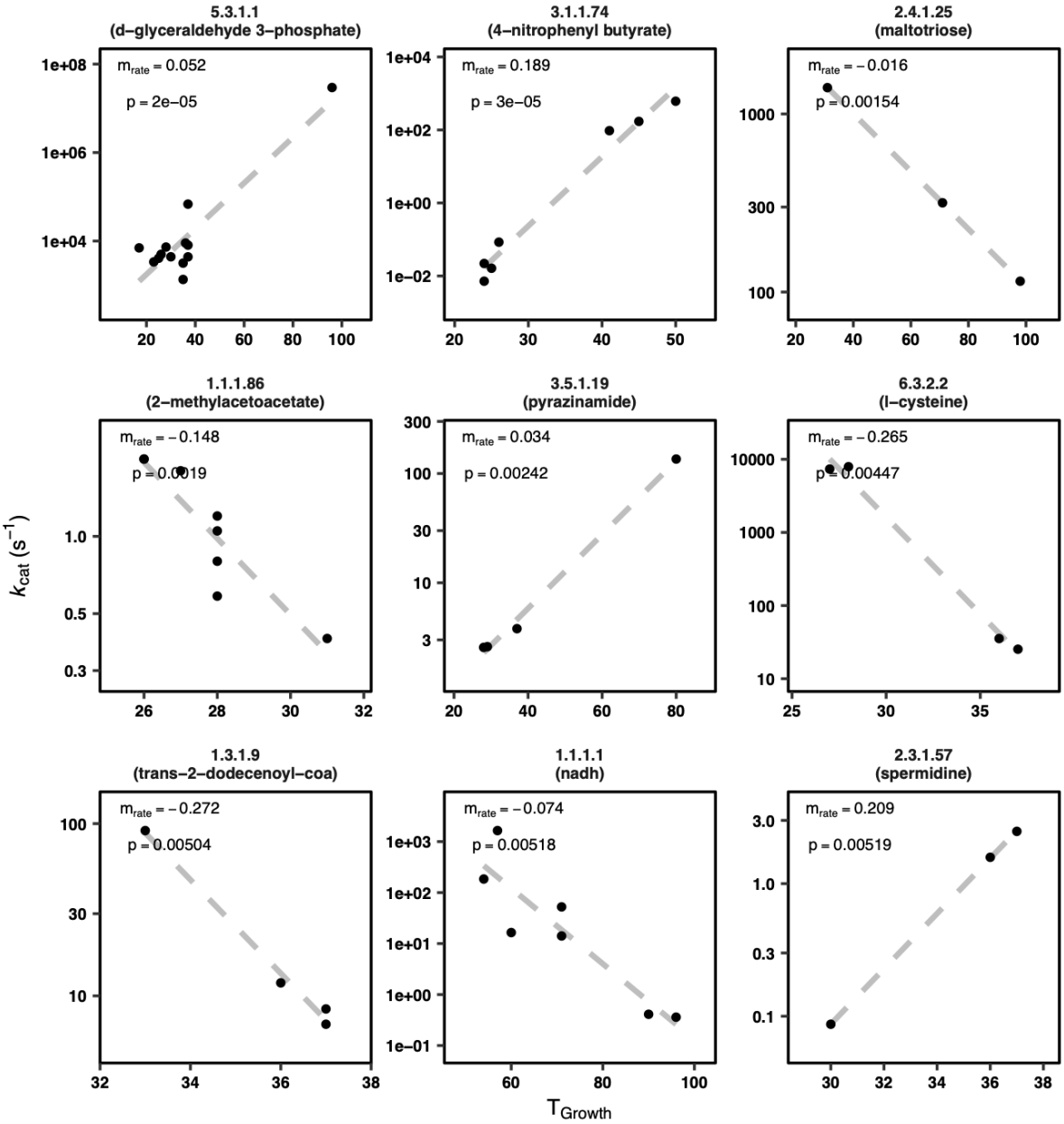

Figure 2—figure supplement 3: Example m_{rate} plots (9 of 951 reactions shown).
Reactions with the rate of constituent variants in order of m_{rate} p-value (for all reactions shown, $p < 5.2 \times 10^{-3}$). m_{rate} is the slope of $\log_{10}(k_{cat})$ *vs.* T_{Growth}. Note different scales for the axes. 5.3.1.1: triose-phosphate isomerase; 3.1.174: cutinase; 2.4.1.25: 4-alpha-glucanotransferase; 1.1.1.86: ketol-acid reductoisomerase; 3.5.1.19: nicotinamidase; 6.3.2.2: glutamate-cysteine ligase; 1.3.1.9: enoyl-[acyl-carrier-protein] reductase (NADH); 1.1.1.1: alcohol dehydrogenase; 2.3.1.57: diamine N-acetyltransferase.

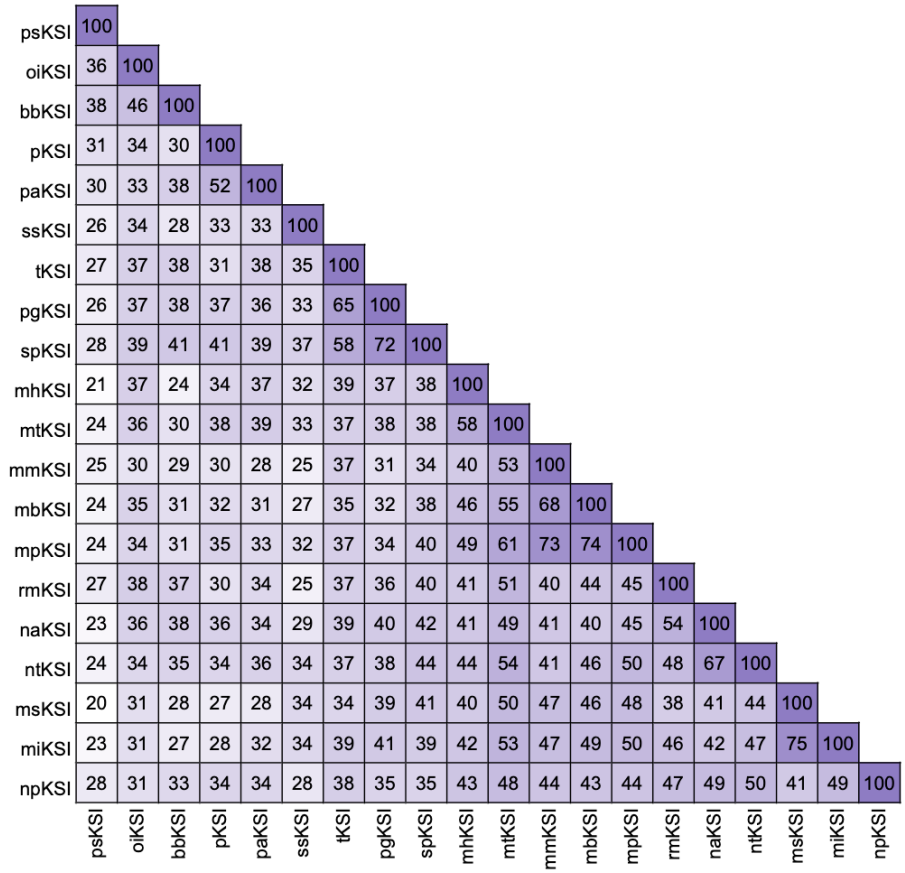

Figure 3—figure supplement 1: KSI variant similarity.
The primary sequence variation of each KSI variant ranges from 20-75% amino acid identity.

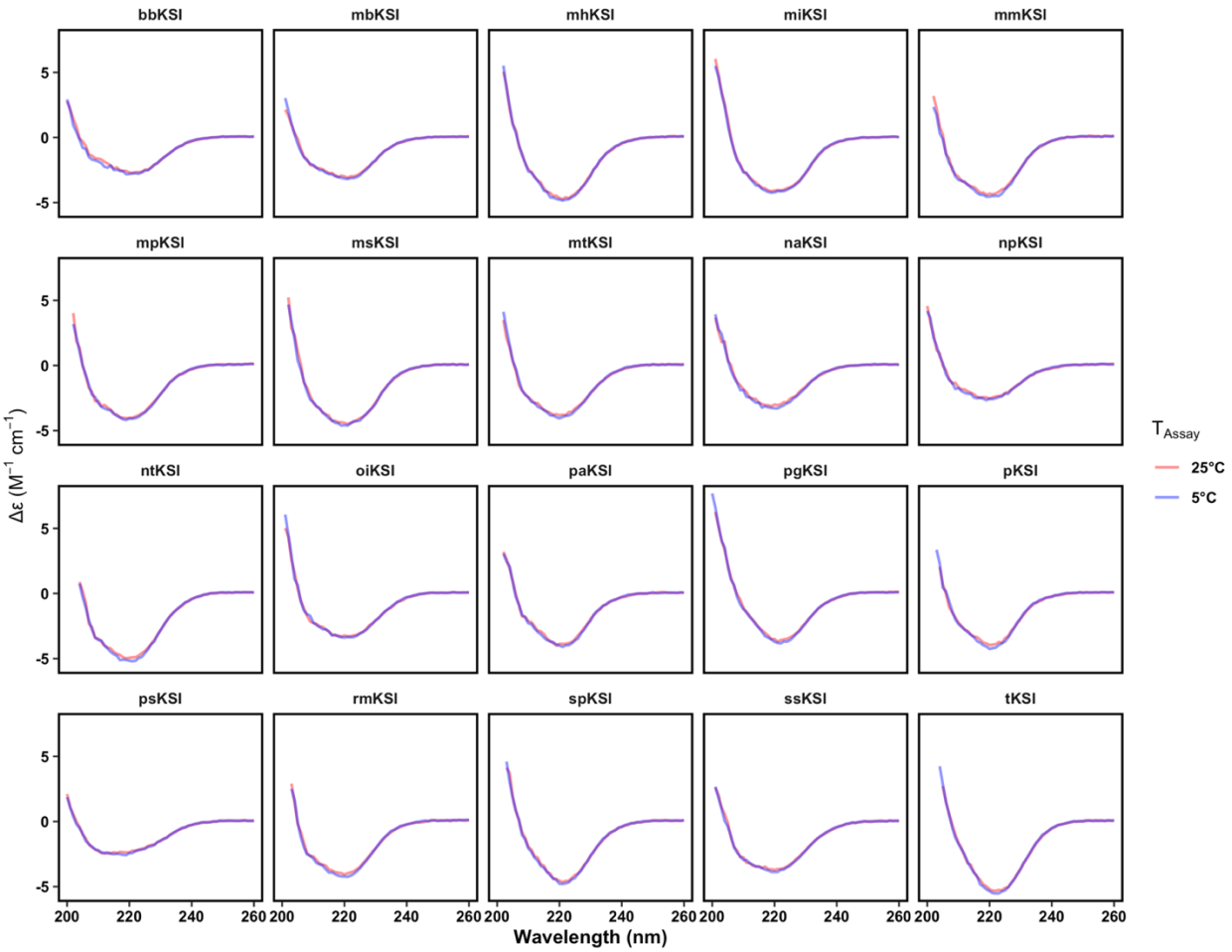

Figure 3—figure supplement 2: KSI variant circular dichroism spectra are similar at cold and warm temperature.
Far ultraviolet circular dichroism (CD) spectra at 5°C (blue) and 25°C (red) are indistinguishable. Measurements for each variant were made at an enzyme concentration of 20 μM.

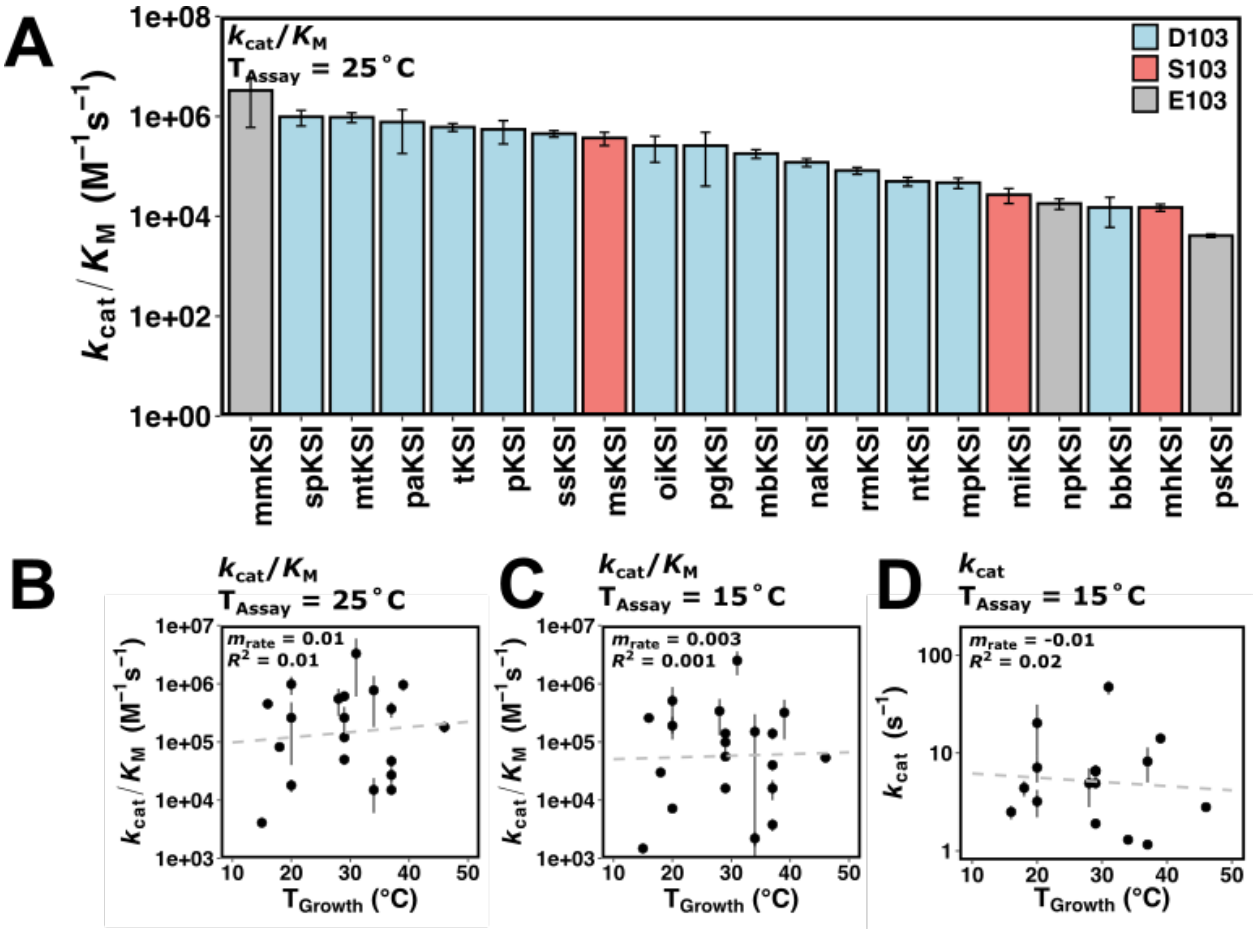

Figure 3—figure supplement 3: Ketosteroid isomerase rates vary with organism growth temperature in k_{cat} and in k_{cat}/K_M.

(A) Rate of KSI variants (k_{cat}/K_M) at a common assay temperature (T_{Assay}) of 25°C. KSI variants with D103 are represented in blue, S103 in red, and E103 in grey (*P. putida* numbering). (B) Rates (k_{cat}/K_M) of KSI variants at 25°C assay temperature (T_{Assay}) *vs.* organism growth temperature (T_{Growth}) (n = 20, m_{rate} = 0.01, R^2 = 0.01, p = 4 ×10^{-7}). (C) Rates (k_{cat}/K_M) of KSI variants at 15°C assay temperature (T_{Assay}) *vs.* organism growth temperature (T_{Growth}) (n = 20, m_{rate} = 0.003, R^2 = 0.001, p = 3 ×10^{-7}). (D) Rates (k_{cat}) of KSI variants at 15°C assay temperature (T_{Assay}) *vs.* organism growth temperature (T_{Growth}) (n = 20, m_{rate} = -0.01, R^2 = 0.02, p = -0.11). Error bars represent standard deviation of at least two different experimental measurements varying [E] at least five-fold (25°C) or two-fold (15°C).

Variant	Organism	Isolation Origin	T_{Growth}[a]	Reference
bbKSI	*Brevibacillus borstelensis*	Soil	34°C	(Shida et al., 1996)
tKSI	*Comamonas testosteroni*	Soil	29°C	(Marcus and Talalay, 1956)
mbKSI	*Mycobacterium botniense*	Streamwater	46°C	(Torkko et al., 2000)
mhKSI	*Mycobacterium hassiacum*	Urine	37°C[b]	(Schröder et al., 1997)
miKSI	*Mycobacterium mantenii*	Lymph node	37°C	(van Ingen et al., 2009)
mmKSI	*Mycobacterium marinum*	Fish tubercles	31°C	(Aronson, 1926)
mpKSI	*Mycobacterium parmense*	Cervical lymph node	37°C	(Fanti et al., 2004)
msKSI	*Mycobacterium simiae*	Rhesus monkey	37°C	(Karassova et al., 1965)
mtKSI	*Mycobacterium thermoresistibile*	Soil	39°C	(Tsukamura, 1966)
naKSI	*Nocardia alba*	Soil	29°C	(Li et al., 2004)
ntKSI	*Nocardia thailandica*	Pus	29°C	(Kageyama et al., 2004)
npKSI	*Nocardioides psychrotolerans*	Glacier	20°C	(Liu et al., 2013)
oiKSI	*Oceanobacillus iheyensis*	Marine sediment	29°C	(Lu et al., 2001)
psKSI	*Paenibacillus antarcticus*	Antarctic sediment	15°C	(Montes et al., 2004)
pgKSI	*Polaromonas glacialis*	Glacier	20°C	(Margesin et al., 2012)
paKSI	*Pseudomonas aeruginosa*	Sliced boiled potatoes	34°C	(Hugh and Leifson, 1964)
pKSI	*Pseudomonas putida*	Soil and water	28°C	(Timmis, 2002)
rmKSI	*Rhodococcus marinonascens*	Marine sediment	18°C	(Helmke and Weyland, 1984)
ssKSI	*Shewanella halifaxensis*	Marine sediment	16°C	(Zhao et al., 2006)
spKSI	*Simplicispira psychrophilia*	Antarctic mosses	20°C	(Terasaki, 1979)

Figure 3—source data 1: KSI origins and organism growth temperatures.

[a] (Engqvist, 2018)

[b] Alternatively reported to grow optimally at 65°C (Schröder et al., 1997). For consistency, curated values from (Engqvist, 2018) are used in this work.

Variant	T_{Growth}[a]	[E]	T_{Assay} (°C)[b]	k_{cat} (s^{-1})[c]	K_M (μM)[c]	k_{cat}/K_M (s^{-1} M^{-1})[c]
bbKSI	34°C	25-500nM	24.7 ± 0.5	1.7 ± 0.2	134 ± 54	(1.5 ± 0.9) × 10^4
tKSI	29°C	0.5-5nM	26.0 ± 1.6	24.9 ± 12.2	40 ± 16	(6.1 ± 1.1) × 10^5
mbKSI	46°C	5-50nM	25.1 ± 0.1	6.9 ± 0.6	40.5 ± 12	(1.8 ± 0.4) × 10^5
mhKSI	37°C	10-500nM	25.2 ± 0.2	1.3 ± 0.1	92 ± 20	(1.5 ± 0.2) × 10^4
miKSI	37°C	5-100nM	24.7 ± 0.8	1.6 ± 0.5	65 ± 37	(2.7 ± 0.9) × 10^4
mmKSI	31°C	0.25-5nM	25.6 ± 1.3	106.3 ± 21.0	45 ± 21	(3.3 ± 2.7) × 10^6
mpKSI	37°C	10-50nM	25.9 ± 1.4	3.4 ± 0.5	76 ± 28	(4.7 ± 1.0) × 10^4
msKSI	37°C	5-50nM	25.0 ± 0.1	29.2 ± 7.7	80 ± 12	(3.7 ± 1.1) × 10^5
mtKSI	39°C	0.5-25nM	26.0 ± 1.3	44.3 ± 7.7	47 ± 4	(9.6 ± 2.1) × 10^5
naKSI	29°C	10-50nM	27.1± 0.6	15.9 ± 3.1	144 ± 52	(1.2 ± 0.2) × 10^5
ntKSI	29°C	10-100nM	26.5 ± 1.2	4.8 ± 1.1	104 ± 49	(5.0 ± 1.0) × 10^4
npKSI	20°C	25-250nM	24.8 ± 0.4	6.8 ± 2.0	368 ± 31	(1.8 ± 0.4) × 10^4
oiKSI	29°C	1-40nM	25.9 ± 0.9	19.2 ± 7.6	107 ± 41	(2.6 ± 1.4) × 10^5
psKSI	15°C	50-500nM	25.0 ± 0.0	1.7 ± 0.0	411 ± 30	(4.1 ± 0.3) × 10^3
pgKSI	20°C	0.5-25nM	26.3 ± 0.9	18.1 ± 8.2	109 ± 86	(2.6 ± 2.2) × 10^5
paKSI	34°C	0.5-15nM	26.8 ± 0.5	9.4 ± 2.3	21 ± 18	(7.7 ± 5.9) × 10^5
pKSI	28°C	1.5-15nM	25.7 ± 1.1	11.2 ± 3.1	25 ± 13	(5.5 ± 2.7) × 10^5
rmKSI	18°C	5-50nM	25.0 ± 0.0	10.3 ± 2.7	125 ± 13	(8.2 ± 1.2) × 10^4
ssKSI	16°C	5-50nM	24.6 ± 0.6	8.7 ± 2.5	19 ± 3	(4.4 ± 0.7) × 10^5
spKSI	20°C	0.5-10nM	26.4 ± 0.4	70.1 ± 21.6	77 ± 27	(9.8 ± 3.4) × 10^5

Figure 3—source data 2: Kinetic measurement of KSIs at 25˚C with substrate 5(10)-estrene-3,17-dione.

[a] (Engqvist, 2018)

[b] Reported assay temperatures are the average of at least three measurements per experiment.

[c] average ± standard deviation from 2–9 independent experiments with enzyme concentration varied by at least 5-fold. Values measured with substrate concentrations from 9-600 μM. Value of k_{cat}/K_M are less than 10^7 M^{-1} s^{-1} and thus unlikely to be limited by substrate binding. Reported assay temperatures are the average of at least 3 measurements per experiment.

Variant	T_{Growth}[a]	[E]	T_{Assay} (°C)[b]	k_{cat} (s^{-1})[c]	K_M (μM)[c]	k_{cat}/K_M (s^{-1} M^{-1})[c]
bbKSI	34°C	250-500nM	14.9 ± 0.2	0.27 ± 0.23	115 ± 77	(2.2 ± 0.6) × 10^3
tKSI	29°C	5-100nM	15.3 ± 0.6	4.9 ± 0.3	35 ± 1	(1.4 ± 0.1) × 10^5
mbKSI	46°C	50-100nM	15.3 ± 0.0	2.8 ± 0.2	52 ± 5	(5.3 ± 0.1) × 10^4
mhKSI	37°C	250-500nM	14.9 ± 0.2	0.6 ± 0.3	160 ± 102	(3.8 ± 0.9) × 10^3
miKSI	37°C	50-100nM	14.7 ± 0.1	0.42 ± 0.05	10.6 ± 0.9	(4.0 ± 0.8) × 10^4
mmKSI	31°C	2.5-5nM	15.0 ± 0.3	47.1 ± 7.6	21.2 ± 7.3	(2.5 ± 1.1) × 10^6
mpKSI	37°C	25-50nM	15.0 ± 0.0	1.16 ± 0.02	77 ± 30	(1.6 ± 0.6) × 10^4
msKSI	37°C	25-50nM	15.0 ± 0.1	8.2 ± 3.2	62 ± 39	(1.4 ± 0.3) × 10^5
mtKSI	39°C	5-15nM	15.2 ± 0.2	14.1 ± 1.6	53 ± 29	(3.2 ± 2.1) × 10^5
naKSI	29°C	25-50nM	14.9 ± 0.0	6.5 ± 1.0	116 ± 16	(5.6 ± 0.1) × 10^4
ntKSI	29°C	5-250nM	15.5 ± 0.6	1.9 ± 0.2	120 ± 21	(1.6 ± 0.1) × 10^4
npKSI	20°C	100-250nM	14.9 ± 0.2	3.2 ± 1.0	446 ± 116	(7.2 ± 0.4) × 10^3
oiKSI	29°C	1-50nM	15.3 ± 0.4	6.6 ± 0.4	73 ± 25	(9.9 ± 3.8) × 10^4
psKSI	15°C	250-500nM	15.3 ± 0.0	0.7 ± 0.1	500 ± 62	(1.5 ± 0.1) × 10^3
pgKSI	20°C	2.5-50nM	15.3 ± 0.8	6.8 ± 1.5	43 ± 9	(1.7 ± 0.7) × 10^5
paKSI	34°C	5-20nM	15.2 ± 0.3	1.3 ± 1.1	11 ± 5	(1.5 ± 1.5) × 10^5
pKSI	28°C	5-25nM	14.4 ± 1.0	4.9 ± 2.1	20 ± 13	(3.4 ± 2.1) × 10^5
rmKSI	18°C	25-50nM	15.4 ± 0.1	4.4 ± 0.8	147 ± 28	(3.0 ± 0.0) × 10^4
ssKSI	16°C	25-50nM	15.7 ± 0.2	2.5 ± 0.4	10 ± 1	(2.6 ± 0.2) × 10^5
spKSI	20°C	5-10nM	15.3 ± 0.3	20.2 ± 11.0	42 ± 8	(5.1 ± 3.7) × 10^5

Figure 3—source data 3: Kinetic measurement of KSIs at 15˚C with substrate 5(10)-estrene-3,17-dione.

[a] (Engqvist, 2018)

[b] Reported assay temperatures are the average of at least three measurements per experiment.

[c] average ± standard deviation from 2–4 independent experiments with enzyme concentration varied by at least 2-fold. Values measured with substrate concentrations from 9-600 μM.

Trait	Model	Highlighted experimental observations	References
Flexibility (general)	Higher flexibility overcomes reduced motion at lower temperature, allowing enhanced catalysis.	Fish lactate dehydrogenase rate (k_{cat}) correlates with average body temperature. Mollusk cytosolic malate dehydrogenase substrate affinity (K_M) correlates with habitat temperature. Psychrophile α-amylase variant is faster than mesophilic and thermophilic variants. Chitobiase engineering stabilizes and reduces activity of psychrophilic enzyme.	(Feller and Gerday, 2003; Fields et al., 2015)
Flexibility (specific)	Surface flexibility decreases enthalpy and entropy activation terms, reducing temperature dependence of reaction.	Computational methods including molecular dynamics and empirical valence bond simulations of diverse enzyme systems, with specific focus on citrate synthase and trypsin variants, suggest importance of flexibility of surface residues in cold adaptation.	(Åqvist et al., 2017)
Heat capacity modulation	Altered temperature dependence of reaction reduces rate decrease as temperature is lowered	More negative $\Delta C_p^{\ddagger}$ has been observed in psychrophilic isopropylmalate dehydrogenase and α-glucosidase. In contrast, more negative $\Delta C_p^{\ddagger}$ has also been suggested as a driver of adaptation to higher temperature in reconstructed ancestral adenylate kinase sequences.	(Arcus et al., 2016; Nguyen et al., 2017)
Dynamic allostery	Partial unfolding arising from conformational entropy-enhancing mutation can affect k_{cat} and K_M	Dynamics-based regulation arising from mutations distal to the active site of mesophilic adenylate kinase affect substrate affinity and turnover, suggesting a mechanism of cold adaptation.	(Saavedra et al., 2018)

Supplementary file 1—Overview of proposed molecular models of cold adaptation.

Variant	Species	T_{Growth}*	Pos. 16	Pos. 103	Pos. 40	Pos. 86	Pos. 120	Pos. 57	Pos. 32	Sequence
pKSI	*Pseudomonas putida*	28	Y	D	D	F	W	Y	Y	MNLPTAQEVQGLMARYIELVD VGDIEAIVQMYADDATVEDPF GQPPIHGREQIAAFYRQGLGGG KVRACLTGPVRASHNGCGAM PFRVEMVWNGQPCALDVIDV MRFDEHGRIQTMQAYWSEVN LSVREPQ
tKSI	*Comamonas testosteroni*	29	Y	D	D	F	F	Y	F	MNTPEHMTAVVQRYVAALNA GDLDGIVALFADDATVEDPVG SEPRSGTAAIREFYANSLKLPL AVELTQEVRAVANEAAFAFTV SFEYQGRKTVVAPIDHFRFNGA GKVVSMRALFGEKNIHAGA
mhKSI	*Mycobacterium hassiacum*	37	Y	S	D	W	W	Y	Y	MSTPQDNANTVHRYLEFVAKG QPDEIAALYADDATVEDPVGS EVHIGRQAIRGFYGNLENVQSR TEVKTLRALGHEVAFYWTLSI GGDEGGMTMDIISVMTFNDDG RIKSMKAYWTPENITQR
mtKSI	*Mycobacterium thermoresistibile*	39	Y	D	D	F	W	Y	Y	MTTVPDKTAAITDTVHRYLEL VAQGRADEITELYADDATVED PVGSDVHVGRQSIRKFYGNIEN IKARTELLTLRVCGNEAAFLFR LEMDLGDNTMTIEPIDVMVFD ADGRIASMKAYWN
oiKSI	*Oceanobacillus iheyensis*	29	Y	D	D	F	W	F	F	MPTEQEMKASLQKYLEGFNEG NSEKVISLFAEDARVEDPVGSE PLKGKASITTFFQQAIPSVKRLE LAAPIRGSHGNAAAMAFNIYV EMEGKGAVIRCIDVMTFNDDG FIIDMKAYWGPEDVQS
spKSI	*Simplicispira psychrophilia*	20	Y	D	D	F	F	Y	Y	MPTPEHMQAAVRAYIAALNA GDIDAIVALYAEDATVEDPVG ATPQRGLAEIRRFYSASLQMQL QVVLEGPVRAVANEAAFAFSV ALVMDGQRLTIRPIDVMRFDD AGRITAMRAFFGPSNISHG
pgKSI	*Polaromonas glacialis*	20	Y	D	D	F	F	Y	Y	MPTPEHMQATVEAYVRALNA SDLDAIVALYADDAVVEDPVG TAPKRGLAEIRAFYAGSLKLKL RVELEGQIRAVASEAAFAFSVS FEVKGQRTTIRPIDLFRFDDAG RIVQMRAFFGPANISAD
paKSI	*Pseudomonas aeruginosa*	34	Y	D	D	F	W	Y	Y	MISPQQVQEIMTRYVELVDAC DIDGILALYARDALVEDPVGSP PHVGIEAVGRFYRNGLGRANA RARRTGPVSASHAGSGAVPFC VDLEWNGRACSIQVIDVMEFD AGGLICSMKAYWGEANVVGR DAP
bbKSI	*Brevibacillus borstelensis*	34	Y	D	D	F	W	F	F	MNNSPMMKQALLAYVDAFNA GDAERLLALFAEEATVEDPVG LEPKRGRAEFEQFFRYAISGGA KLELVAPPRASFSNHAAVTFIV HTEMEGRAVGIHVTDVMTFDE NGKIVHMRAFWGQDDVRTAD SPNA
msKSI	*Mycobacterium simiae*	37	Y	S	D	W	W	Y	Y	MPSPEAITQTVNSYLTLLAKGA TDEIVNLYTTDATIEDPIGADVL

										RGHDAVRAFYTAIQDAKKETE LAEIRIGGNEAAFLWHLTLDAG DSRTRISPISVMTFDDQARVAS MRAFWSPSDVRVL
miKSI	*Mycobacterium mantenii*	37	Y	S	D	W	W	Y	Y	MPSPEAITETVNRYLALVATGT ADEIVTLYAADATIEDPIGSDIR RGHDAIRGFYAGFQDAKKDTE LAELRISGSEAAFLWHLTLDAG DSRTRISPISTMSFDGDAKITSM RAFWSPADVQVL
mmKSI	*Mycobacterium marinum*	31	Y	E**	D	F	W	Y	Y	MPNSAERSQAITETVNRYMSV LADGDADDLVGFYADDATLE DPVGGEVHIGTRAIHGFYSAIA GLTRECELVSLRVCGNEAAFQ FRLTVTSGDSKMRVEPIEVMVF DRSGKVAAMKAYWSAADVTH L
mpKSI	*Mycobacterium parmense*	37	Y	D	D	F	W	Y	Y	MRNAADRVQAITDTVNRYIEL VAKGSADDLVELYADDATVE DPVGGEVHIGRQAIHGFYSAV DGVARECELVSLRVAGNEAAF LFRLTVTAGDHRMVIEPIDVM VFDDRGKVTAMKAYWSAANV TQG
npKSI	*Nocardioides psychrotolerans*	20	Y	E**	D	F	W	Y	Y	MVAPNADIRSTVQRYLDLVAD GTSTEIVALYAPDATLEDPVGS EVLRGREAIGGFYAGLDGLAM TTNLVTLRVCAGHAAFHFEVV TDTGGMKFKMAPLEVMTFDG DGLITSMRAFWSDEDLVVDA
naKSI	*Nocardia alba*	29	Y	D	D	F	W	Y	Y	MASADDIRATVRKYVEAVGSG TAADVVALYREDATVEDPVGT EPHVGHAAITKFYENIEPLQRS TELFSVRVAGDSAAFSFRVVTT FGEQTFTLDPIDVMTFDEDARI VSMRAFWSQDDMVVG
ntKSI	*Nocardia thailandica*	29	Y	D	D	L**	W	Y	Y	MASPDDIRATVRRYVELVGTG TAADIAALYTEDATVEDPVGS APHTGRAAIEKFYGALDGTTR HTELLTVRVAGDNAAFGLRVV TRAGDKTITIEPIDVMTFDADA RITGMRAFWSASDIAFG
mbKSI	*Mycobacterium botniense*	46	Y	D	D	F	W	Y	Y	MRSAPERTQAITNAVHRYLGL LANGSVDDLVEMYAADATVE DPVGGEVHIGRQAIRSFYSALD GAERDCELVSLRVAGNEAAFQ FRLTVATGGSVVRIEPIDVMAF ADDGKVTAMKAYWSAADVT QLGSGDEAVRSGPGQSG
ssKSI	*Shewanella halifaxensis*	16	Y	D	D	F	W	Y	Y	MITEQFGLGVVSSYIEFLNNGN FEGIASLYSKNAIIEDPIGSDKII GRTAIQDFYRQAVLGVHQVNQ LGEVRVASNEIAFPFEVVLAKD PNLAISVIDIFKINAEGEIDSMR AFWGPGNVKSVSKPAPITA
psKSI	*Paenibacillus antarcticus*	15	Y	E**	D	I**	W	Y	F	MLEQPEIKQAMQQYIDHFNAN DLESLLGLFSETASLEDPVGSIP IEGTEPIRQFYSKVVNGDTKIKL MTPICGSHSHSGAMAIEIETNA KGEKVVIQAIEIMSFDEFGKIM NLQVYWGKEDLNFS

rmKSI	*Rhodococcus marinonascens*	18	Y	D	D	F	W	Y	Y	MAPSAADIRKIVERYVAAVAT GTADDVLSLYAEGATVEDPVG TEPRTSVDSLREFYSVLEPMKQ TGELLTLRIAGNSAAFHFSLVT DLGEQKFEIAPIDVMTFDDDGK ITSMKAYWGQDDMITRAD
	(*) From Engqvist 2018									
	(**) Novel active site feature not described in characterized KSIs previously (*P. putida*) numbering									

Supplementary File 2—KSI sequences.

Supplementary References

Åqvist J, Isaksen GV, Brandsdal BO. 2017. Computation of enzyme cold adaptation. *Nat Rev Chem* **1**:0051. doi:10.1038/s41570-017-0051

Arcus VL, Prentice EJ, Hobbs JK, Mulholland AJ, Van der Kamp MW, Pudney CR, Parker EJ, Schipper LA. 2016. On the Temperature Dependence of Enzyme-Catalyzed Rates. *Biochemistry* **55**:1681–1688. doi:10.1021/acs.biochem.5b01094

Aronson J. 1926. Spontaneous Tuberculosis in Salt Water Fish. *J Infect Dis* **39**:315–320.

Engqvist MKM. 2018. Correlating enzyme annotations with a large set of microbial growth temperatures reveals metabolic adaptations to growth at diverse temperatures. *BMC Microbiol* **18**:177. doi:10.1186/s12866-018-1320-7

Fanti F, Tortoli E, Hall L, Roberts GD, Kroppenstedt RM, Dodi I, Conti S, Polonelli L, Chezzi C. 2004. Mycobacterium parmense sp. nov. *Int J Syst Evol Microbiol* **54**:1123–1127. doi:10.1099/ijs.0.02760-0

Feller G, Gerday C. 2003. Psychrophilic enzymes: hot topics in cold adaptation. *Nat Rev Microbiol* **1**:200–208. doi:10.1038/nrmicro773

Fields PA, Dong Y, Meng X, Somero GN. 2015. Adaptations of protein structure and function to temperature: there is more than one way to "skin a cat." *J Exp Biol* **218**:1801–1811. doi:10.1242/jeb.114298

Helmke E, Weyland H. 1984. Rhodococcus marinonascens sp. nov., an Actinomycete from the Sea. *Int J Syst Bacteriol* **34**:127–138. doi:10.1099/00207713-34-2-127

Hugh R, Leifson E. 1964. The proposed Neotype Strains of Pseudomonas Aeruginosa (Schroeter 1872) Migula 1900. *Int Bull Bacteriol Nomencl Taxon* **14**:69–84. doi:10.1099/0096266X-14-2-69

Kageyama A, Poonwan N, Yazawa K, Suzuki S, Kroppenstedt RM, Mikami Y. 2004. Nocardia vermiculata sp. nov. and Nocardia thailandica sp. nov. Isolated from Clinical Specimens. *Actinomycetologica* **18**:27–33. doi:10.3209/saj.18_27

Karassova V, Weissfeiler J, Krasznay E. 1965. Occurrence of atypical mycobacteria in Macacus rhesus. *Acta Microbiol Acad Sci Hung* **12**:275–282.

Li W-J, Jiang Y i., Kroppenstedt RM, Xu L-H, Jiang C-L. 2004. Nocardia alba sp.nov., a Novel Actinomycete Strain Isolated from Soil in China. *Syst Appl Microbiol* **27**:308–312. doi:10.1078/0723-2020-00270

Liu Q, Xin Y, Liu H, Zhou Y, Wen Y. 2013. Nocardioides szechwanensis sp. nov. and Nocardioides psychrotolerans sp. nov., isolated from a glacier. *Int J Syst Evol Microbiol* **63**:129–133. doi:10.1099/ijs.0.038091-0

Lu J, Nogi Y, Takami H. 2001. Oceanobacillus iheyensis gen. nov., sp. nov., a deep-sea extremely halotolerant and alkaliphilic species isolated from a depth of 1050 m on the Iheya Ridge. *FEMS Microbiol Lett* **205**:291–297. doi:10.1111/j.1574-6968.2001.tb10963.x

Marcus PI, Talalay P. 1956. Induction and purification of alpha- and beta-hydroxysteroid dehydrogenases. *J Biol Chem* **218**:661–674.

Margesin R, Spröer C, Zhang D-C, Busse H-J. 2012. Polaromonas glacialis sp. nov. and Polaromonas cryoconiti sp. nov., isolated from alpine glacier cryoconite. *Int J Syst Evol Microbiol* **62**:2662–2668. doi:10.1099/ijs.0.037556-0

Montes MJ, Mercadé E, Bozal N, Guinea J. 2004. Paenibacillus antarcticus sp. nov., a novel psychrotolerant organism from the Antarctic environment. *Int J Syst Evol Microbiol* **54**:1521–1526. doi:10.1099/ijs.0.63078-0

Nguyen V, Wilson C, Hoemberger M, Stiller JB, Agafonov RV, Kutter S, English J, Theobald DL, Kern D. 2017. Evolutionary drivers of thermoadaptation in enzyme catalysis. *Science* **355**:289–294. doi:10.1126/science.aah3717

Saavedra HG, Wrabl JO, Anderson JA, Li J, Hilser VJ. 2018. Dynamic allostery can drive cold adaptation in enzymes. *Nature* **558**:324–328. doi:10.1038/s41586-018-0183-2

Schröder KH, Naumann L, Kroppenstedt RM, Reischl U. 1997. Mycobacterium hassiacum sp. nov., a new rapidly growing thermophilic mycobacterium. *Int J Syst Bacteriol* **47**:86–91. doi:10.1099/00207713-47-1-86

Shida O, Takagi H, Kadowaki K, Komagata K. 1996. Proposal for Two New Genera, Brevibacillus gen. nov. and Aneurinibacillus gen. nov. *Int J Syst Bacteriol* **46**:939–946. doi:10.1099/00207713-46-4-939

Terasaki Y. 1979. Transfer of Five Species and Two Subspecies of Spirillum to Other Genera (Aquaspirillum and Oceanospirillum) , with Emended Descriptions of the Species and Subspecies. *Int J Syst Bacteriol* **29**:130–144.

Timmis KN. 2002. Pseudomonas putida: a cosmopolitan opportunist par excellence. *Environ Microbiol* **4**:779–781. doi:10.1046/j.1462-2920.2002.00365.x

Torkko P, Suomalainen S, Iivanainen E, Suutari M, Tortoli E, Paulin L, Katila ML. 2000. Mycobacterium xenopi and related organisms isolated from stream waters in Finland and description of Mycobacterium botniense sp. nov. *Int J Syst Evol Microbiol* **50**:283–289. doi:10.1099/00207713-50-1-283

Tsukamura M. 1966. Adansonian Classification of Mycobacteria. *J Gen Microbiol* **45**:253–273. doi:10.1099/00221287-45-2-253

van Ingen J, Lindeboom JA, Hartwig NG, de Zwaan R, Tortoli E, Dekhuijzen PNR, Boeree MJ, van Soolingen D. 2009. Mycobacterium mantenii sp. nov., a pathogenic, slowly growing, scotochromogenic species. *Int J Syst Evol Microbiol* **59**:2782–2787. doi:10.1099/ijs.0.010405-0

Zhao J-S, Manno D, Leggiadro C, O'Neil D, Hawari J. 2006. Shewanella halifaxensis sp. nov., a novel obligately respiratory and denitrifying psychrophile. *Int J Syst Evol Microbiol* **56**:205–212. doi:10.1099/ijs.0.63829-0

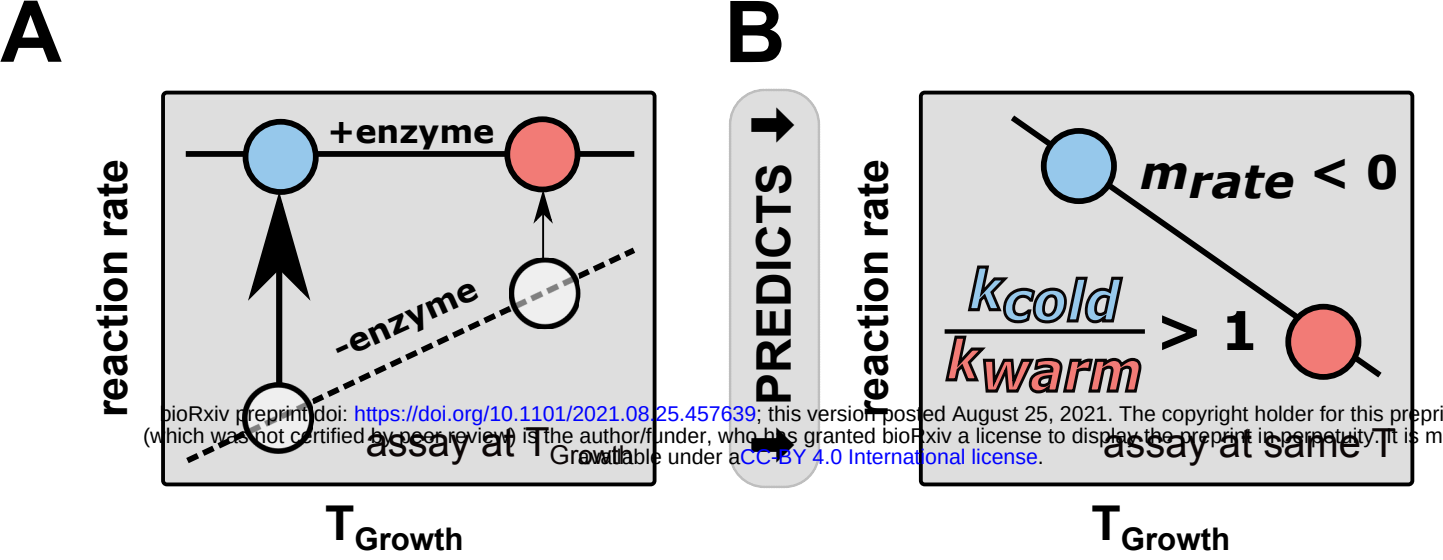

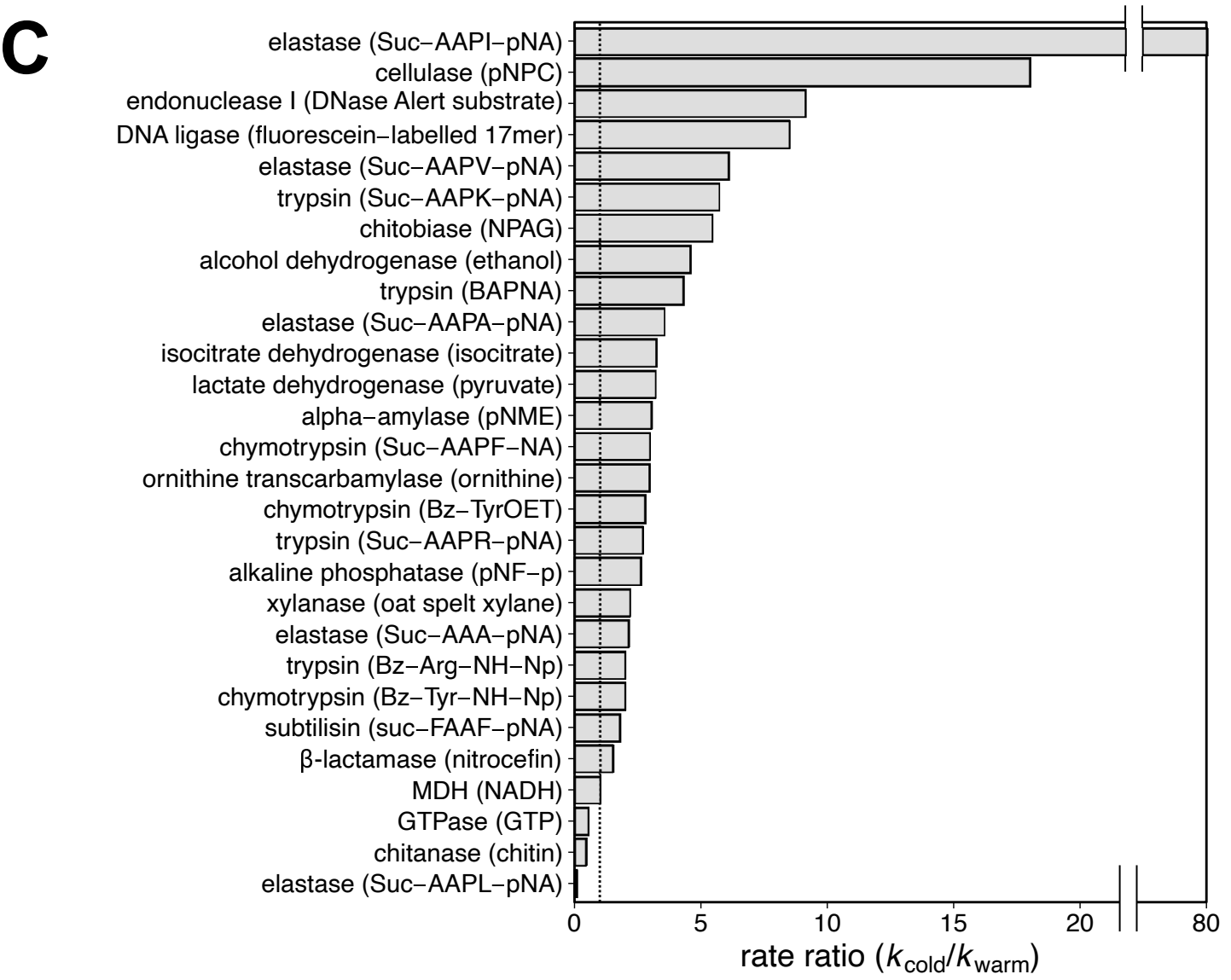

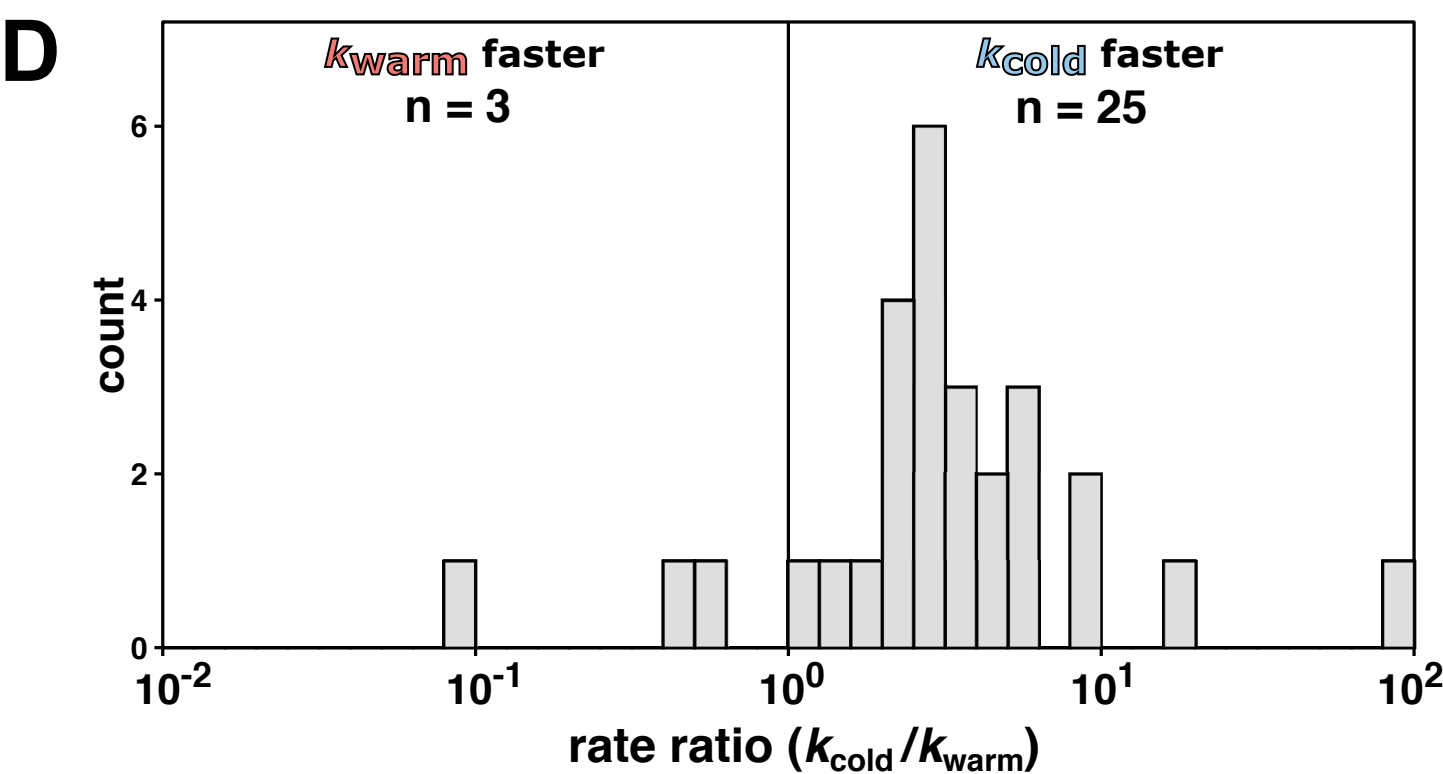

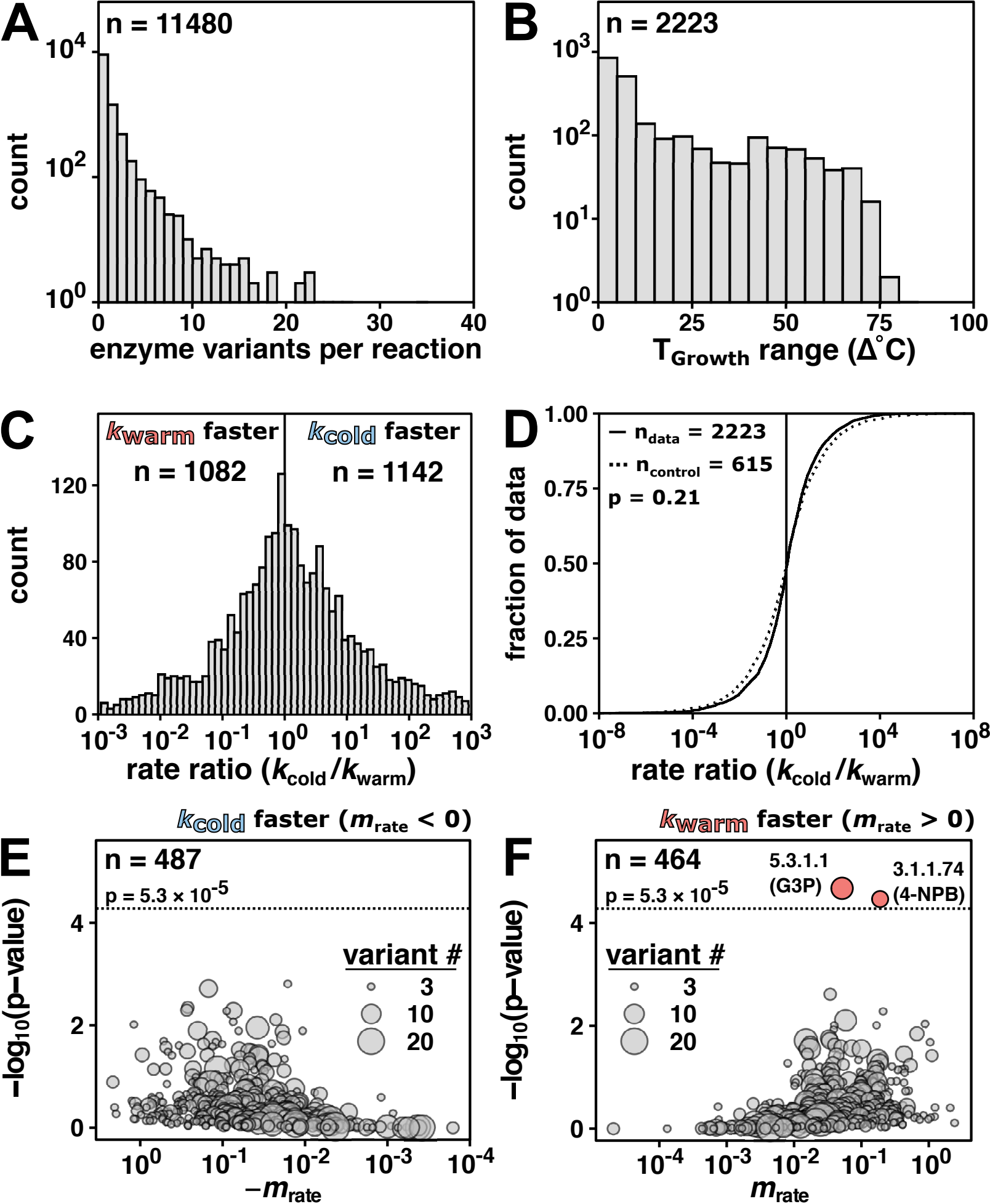
A
n = 11480
count
enzyme variants per reaction
B
n = 2223
count
T_Growth range (Δ°C)
C
k_warm faster
n = 1082
k_cold faster
n = 1142
count
rate ratio (k_cold/k_warm)
D
n_data = 2223
n_control = 615
p = 0.21
fraction of data
rate ratio (k_cold/k_warm)
k_cold faster (m_rate < 0)
E
n = 487
p = 5.3 × 10^-5
variant #
3
10
20
−log10(p−value)
−m_rate
k_warm faster (m_rate > 0)
F
n = 464
p = 5.3 × 10^-5
5.3.1.1 (G3P)
3.1.1.74 (4-NPB)
variant #
3
10
20
−log10(p−value)
m_rate

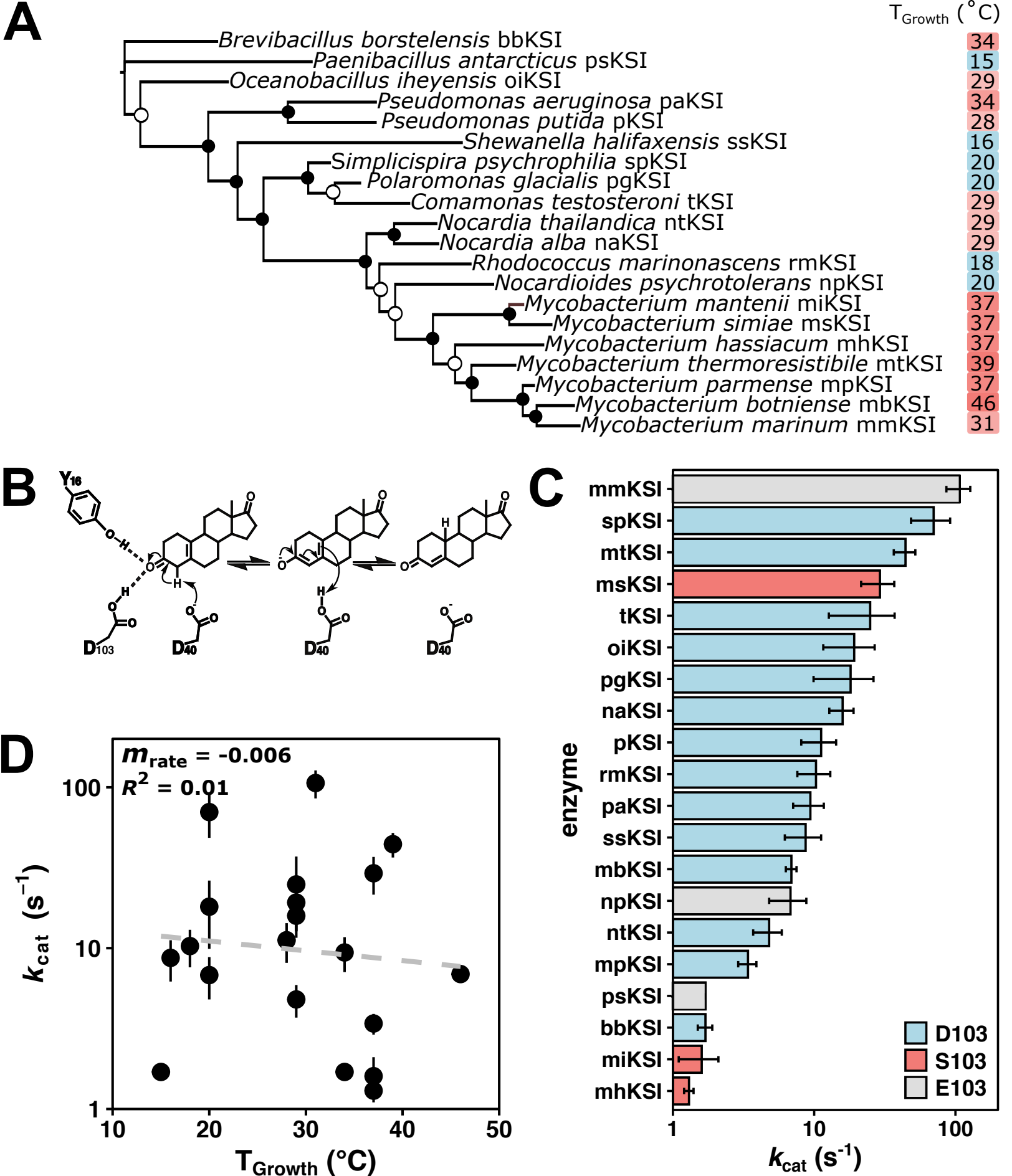
A
T Growth (°C)
Brevibacillus borstelensis bbKSI 34
Paenibacillus antarcticus psKSI 15
Oceanobacillus iheyensis oiKSI 29
Pseudomonas aeruginosa paKSI 34
Pseudomonas putida pKSI 28
Shewanella halifaxensis ssKSI 16
Simplicispira psychrophilia spKSI 20
Polaromonas glacialis pgKSI 20
Comamonas testosteroni tKSI 29
Nocardia thailandica ntKSI 29
Nocardia alba naKSI 29
Rhodococcus marinonascens rmKSI 18
Nocardioides psychrotolerans npKSI 20
Mycobacterium mantenii miKSI 37
Mycobacterium simiae msKSI 37
Mycobacterium hassiacum mhKSI 37
Mycobacterium thermoresistibile mtKSI 39
Mycobacterium parmense mpKSI 37
Mycobacterium botniense mbKSI 46
Mycobacterium marinum mmKSI 31
B
Y16
D103
D40
D40
D40
C
mmKSI
spKSI
mtKSI
msKSI
tKSI
oiKSI
pgKSI
naKSI
pKSI
rmKSI
paKSI
ssKSI
mbKSI
npKSI
ntKSI
mpKSI
psKSI
bbKSI
miKSI
mhKSI
enzyme
D103
S103
E103
1
10
100
kcat (s-1)
D
mrate = -0.006
R2 = 0.01
100
10
1
kcat (s-1)
10
20
30
40
50
T Growth (°C)

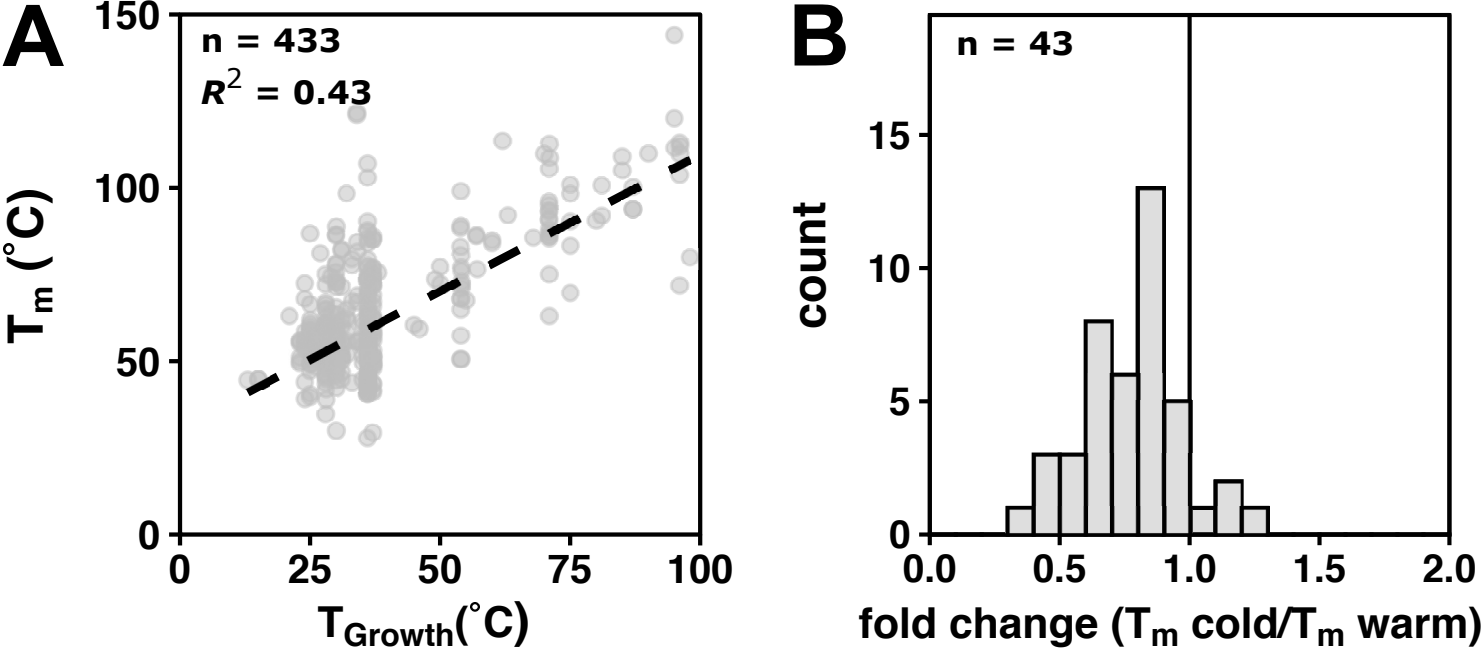
A
n = 433
R^2 = 0.43
T_m (°C)
T_{Growth}(°C)
0
50
100
150
0
25
50
75
100
B
n = 43
count
0
5
10
15
0.0
0.5
1.0
1.5
2.0
fold change (T_m cold/T_m warm)

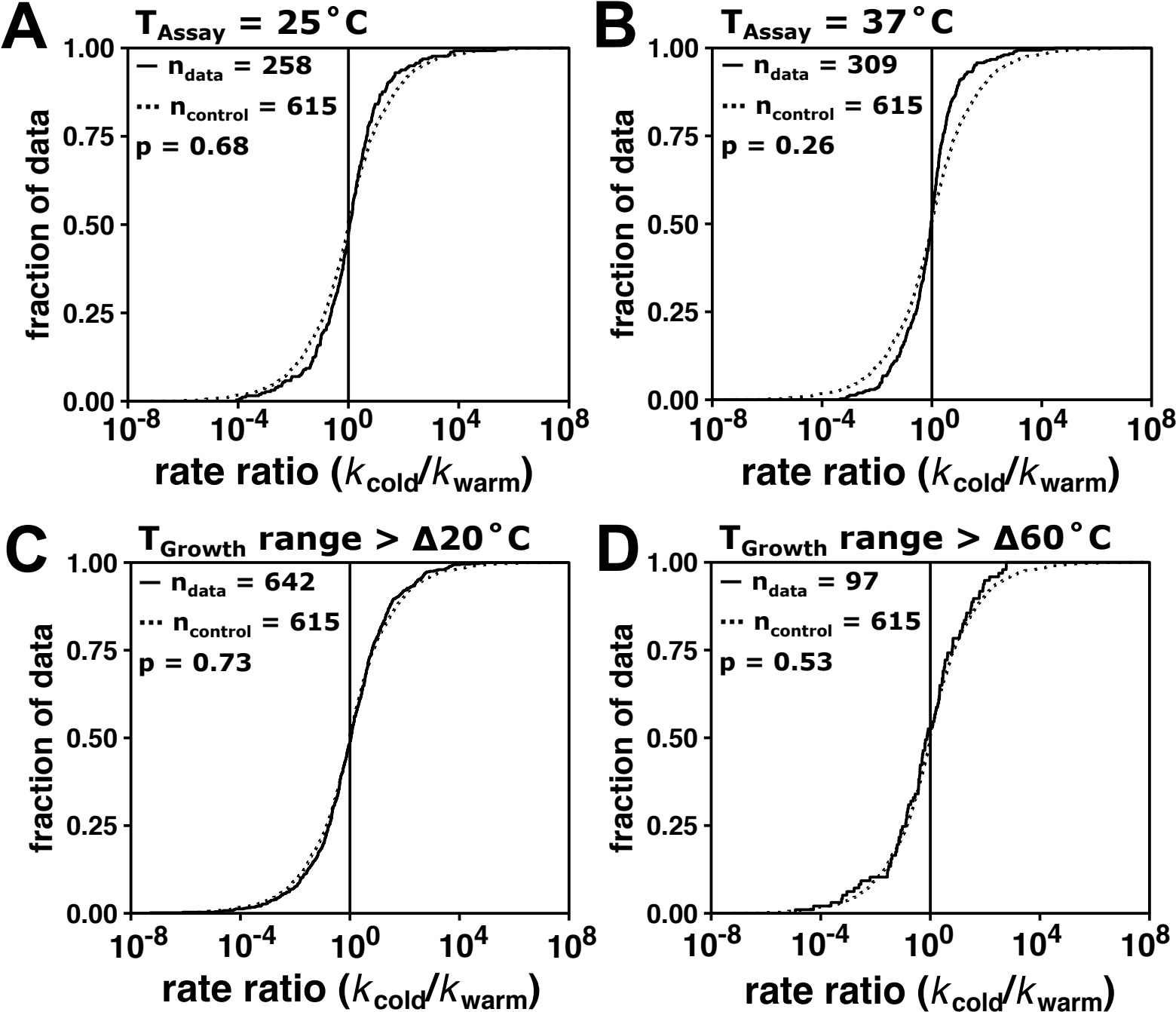
A
T_Assay = 25°C
— n_data = 258
··· n_control = 615
p = 0.68
B
T_Assay = 37°C
— n_data = 309
··· n_control = 615
p = 0.26
C
T_Growth range > Δ20°C
— n_data = 642
··· n_control = 615
p = 0.73
D
T_Growth range > Δ60°C
— n_data = 97
··· n_control = 615
p = 0.53
fraction of data
1.00
0.75
0.50
0.25
0.00
10^-8
10^-4
10^0
10^4
10^8
rate ratio (k_cold/k_warm)

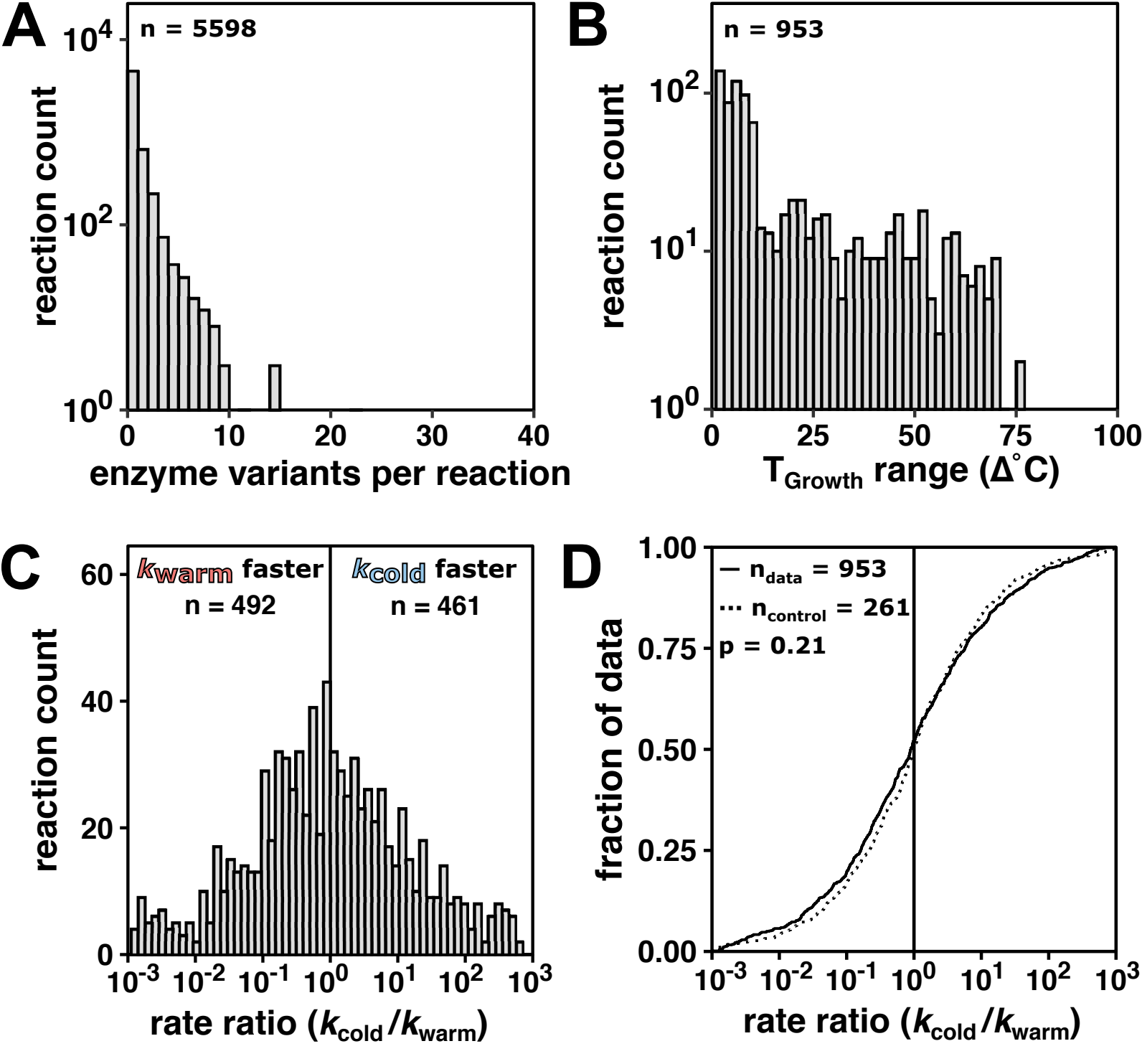
A
n = 5598
reaction count
enzyme variants per reaction
B
n = 953
reaction count
T_Growth range (Δ°C)
C
k_warm faster
n = 492
k_cold faster
n = 461
reaction count
rate ratio (k_cold/k_warm)
D
— n_data = 953
··· n_control = 261
p = 0.21
fraction of data
rate ratio (k_cold/k_warm)

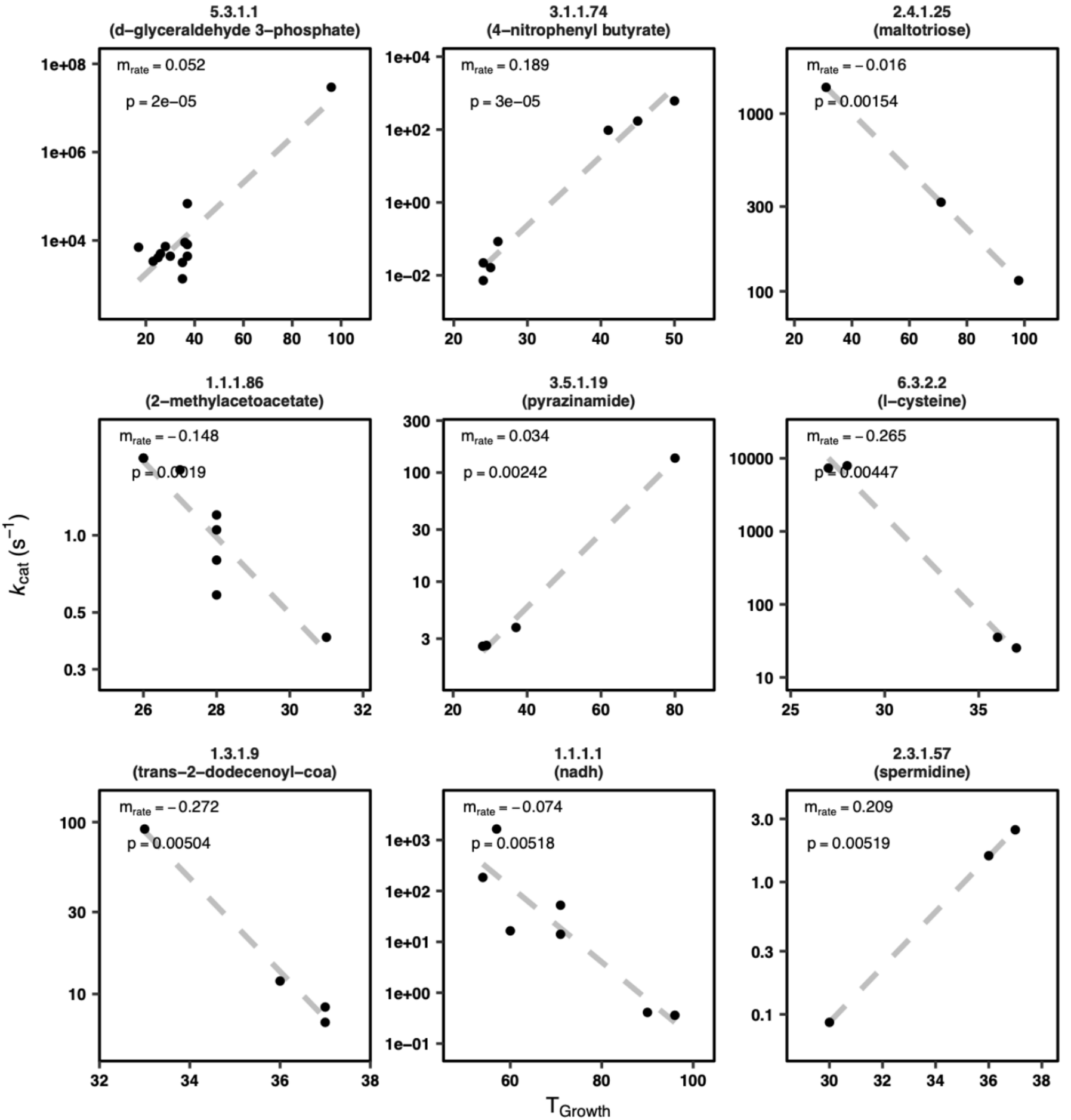

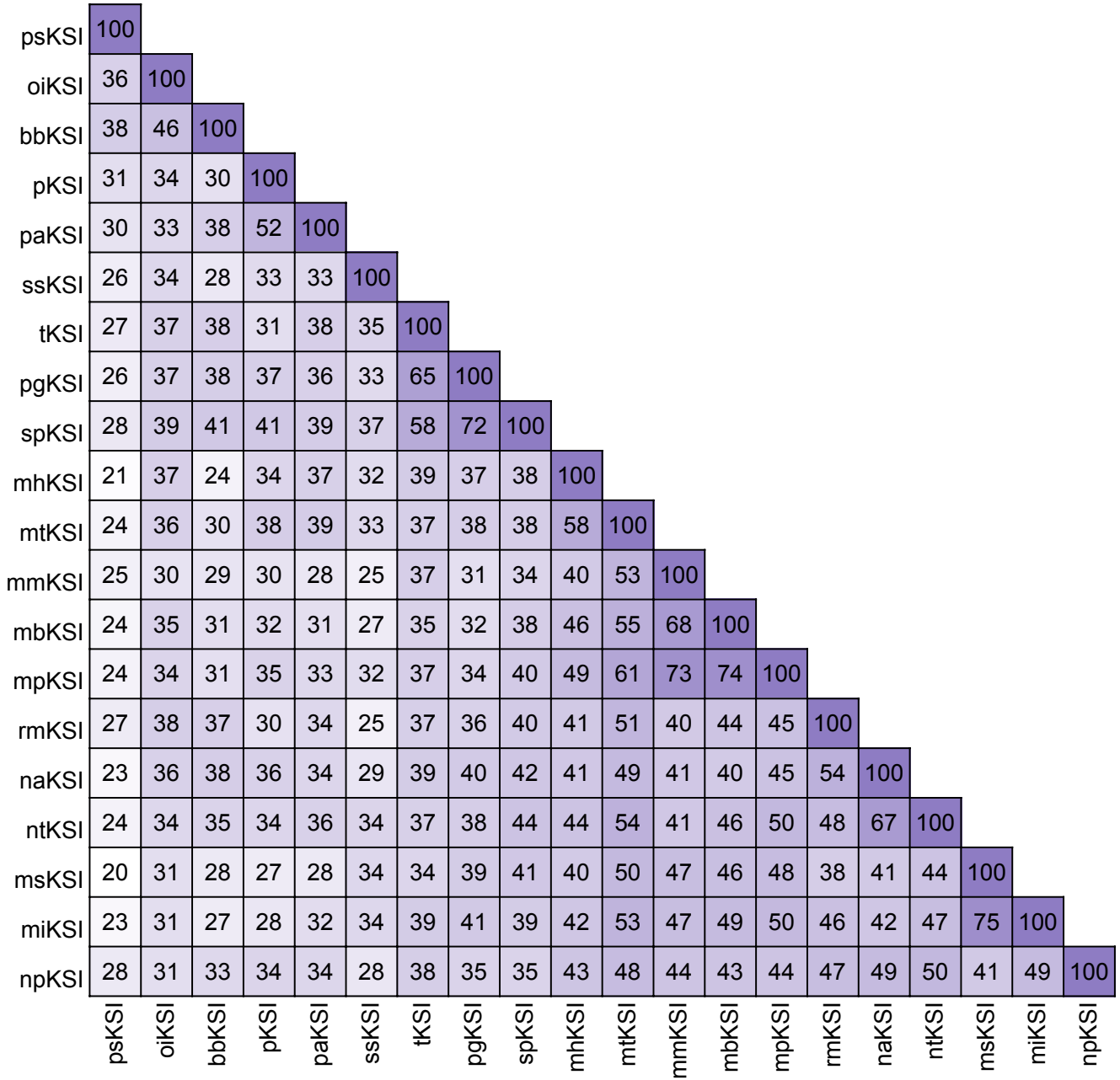
psKSI 100
oiKSI 36 100
bbKSI 38 46 100
pKSI 31 34 30 100
paKSI 30 33 38 52 100
ssKSI 26 34 28 33 33 100
tKSI 27 37 38 31 38 35 100
pgKSI 26 37 38 37 36 33 65 100
spKSI 28 39 41 41 39 37 58 72 100
mhKSI 21 37 24 34 37 32 39 37 38 100
mtKSI 24 36 30 38 39 33 37 38 38 58 100
mmKSI 25 30 29 30 28 25 37 31 34 40 53 100
mbKSI 24 35 31 32 31 27 35 32 38 46 55 68 100
mpKSI 24 34 31 35 33 32 37 34 40 49 61 73 74 100
rmKSI 27 38 37 30 34 25 37 36 40 41 51 40 44 45 100
naKSI 23 36 38 36 34 29 39 40 42 41 49 41 40 45 54 100
ntKSI 24 34 35 34 36 34 37 38 44 44 54 41 46 50 48 67 100
msKSI 20 31 28 27 28 34 34 39 41 40 50 47 46 48 38 41 44 100
miKSI 23 31 27 28 32 34 39 41 39 42 53 47 49 50 46 42 47 75 100
npKSI 28 31 33 34 34 28 38 35 35 43 48 44 43 44 47 49 50 41 49 100
psKSI
oiKSI
bbKSI
pKSI
paKSI
ssKSI
tKSI
pgKSI
spKSI
mhKSI
mtKSI
mmKSI
mbKSI
mpKSI
rmKSI
naKSI
ntKSI
msKSI
miKSI
npKSI

$[E]_{Assay}$ = 20μM

bbKSI | mbKSI | mhKSI | miKSI | mmKSI

mpKSI | msKSI | mtKSI | naKSI | npKSI

ntKSI | oiKSI | paKSI | pgKSI | pKSI

psKSI | rmKSI | spKSI | ssKSI | tKSI

$\Delta\varepsilon$ ($M^{-1}cm^{-1}$)

5
0
-5

200 220 240 260

Wavelength (nm)

T_{Assay}

25°C
5°C

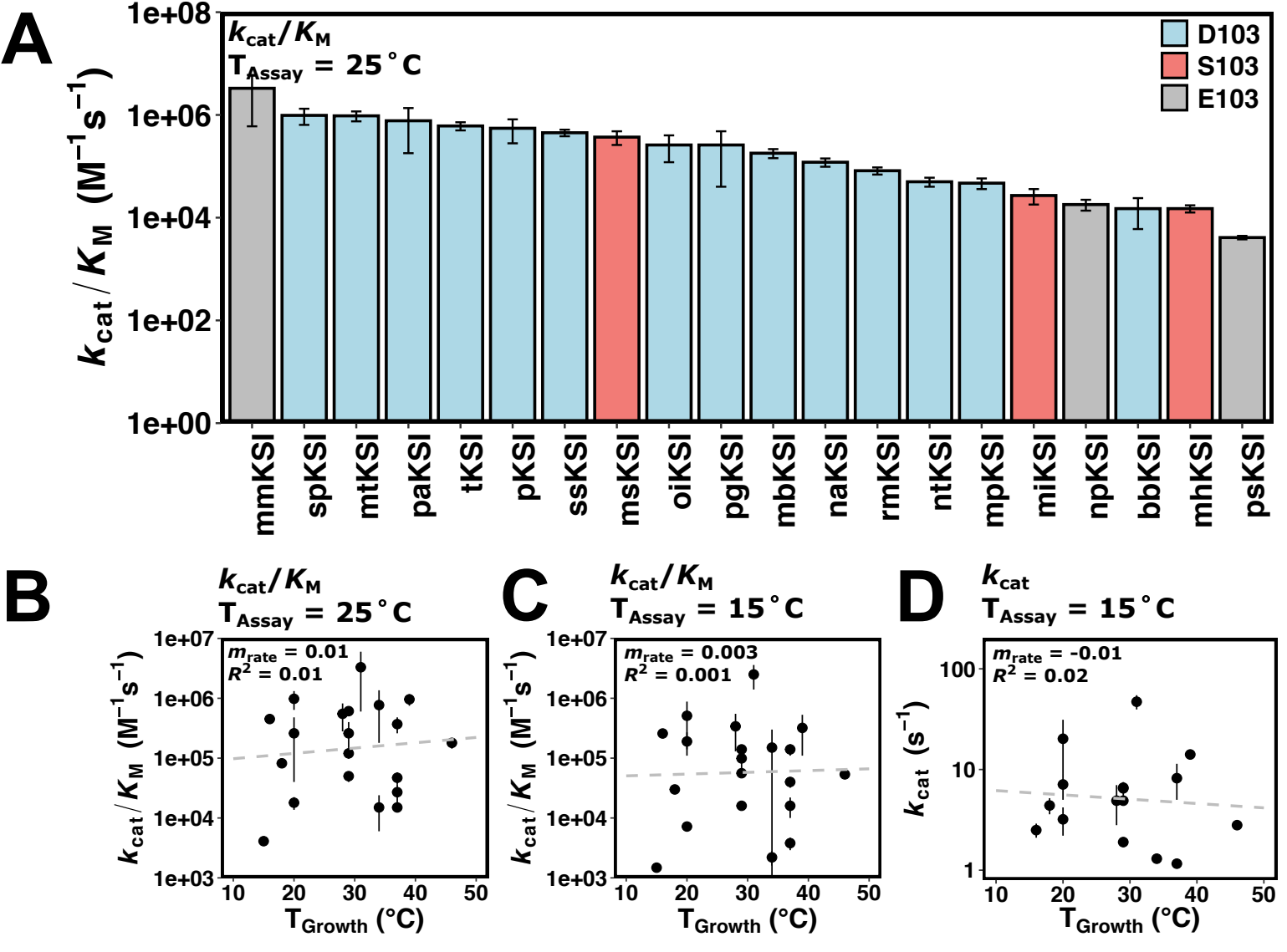
A
k_{cat}/K_M
T_{Assay} = 25 °C
D103
S103
E103
k_{cat}/K_M ($M^{-1}s^{-1}$)
1e+08
1e+06
1e+04
1e+02
1e+00
mmKSI
spKSI
mtKSI
paKSI
tKSI
pKSI
ssKSI
msKSI
oiKSI
pgKSI
mbKSI
naKSI
rmKSI
ntKSI
mpKSI
miKSI
npKSI
bbKSI
mhKSI
psKSI
B
k_{cat}/K_M
T_{Assay} = 25 °C
m_{rate} = 0.01
R^2 = 0.01
k_{cat}/K_M ($M^{-1}s^{-1}$)
1e+07
1e+06
1e+05
1e+04
1e+03
10
20
30
40
50
T_{Growth} (°C)
C
k_{cat}/K_M
T_{Assay} = 15 °C
m_{rate} = 0.003
R^2 = 0.001
k_{cat}/K_M ($M^{-1}s^{-1}$)
1e+07
1e+06
1e+05
1e+04
1e+03
10
20
30
40
50
T_{Growth} (°C)
D
k_{cat}
T_{Assay} = 15 °C
m_{rate} = -0.01
R^2 = 0.02
k_{cat} (s^{-1})
100
10
1
10
20
30
40
50
T_{Growth} (°C)